Received: 24 April 2020 | Revised: 3 October 2020 | Accepted: 30 November 2020

DOI: 10.1111/bph.15344

RESEARCH PAPER

High-content screening identifies inhibitors of oxidative stress-induced parthanatos: cytoprotective and anti-inflammatory effects of ciclopirox

Zsolt Regdon[1,2] | Máté A. Demény[2] | Katalin Kovács[1,3] | Zoltán Hajnády[1,2] | Máté Nagy-Pénzes[1,2] | Edina Bakondi[1] | Alexandra Kiss[1,2] | Csaba Hegedűs[1] | László Virág[1,3]

[1]Department of Medical Chemistry, Faculty of Medicine, University of Debrecen, Debrecen, Hungary

[2]Doctoral School of Molecular Medicine, University of Debrecen, Debrecen, Hungary

[3]MTA-DE Cell Biology and Signaling Research Group, Debrecen, Hungary

Correspondence
László Virag and Csaba Hegedűs, Department of Medical Chemistry, Faculty of Medicine, University of Debrecen, Debrecen, Hungary.
Email: lvirag@med.unideb.hu; hcsaba@med.unideb.hu

Funding information
Emberi Eroforrások Minisztériuma; Hungarian Academy of Sciences, Grant/Award Number: BO/00468/17/8; Nemzeti Kutatási Fejlesztési és Innovációs Hivatal, Grant/Award Numbers: GINOP-2.3.2-15-2016-00020 TUMORDNS, OTKA K112336, OTKA K132193, OTKA PD116845; New National Excellence Program of the Ministry of Human Capacities, Grant/Award Number: ÚNKP-19-4-DE-299

Background and Purpose: Excessive oxidative stress can induce PARP1-mediated programmed necrotic cell death, termed parthanatos. Inhibition of parthanatos may be therapeutically beneficial in a wide array of diseases associated with tissue injury and inflammation. Our goal was to identify novel molecules inhibiting parthanatos.

Experimental Approach: A small library of 774 pharmacologically active compounds was screened in a Sytox Green uptake assay, which identified 20 hits that reduced hydrogen-peroxide-induced parthanatos with an efficiency comparable to the benchmark PARP inhibitor, PJ34.

Key Results: Of these hits, two compounds, antifungal ciclopirox and dopamine receptor agonist apomorphine, inhibited PAR polymer synthesis. These two compounds prevented the binding of PARP1 to oxidatively damaged DNA but did not directly interfere with the interaction between DNA and PARP1. Both compounds inhibited mitochondrial superoxide and H_2O_2 production and suppressed DNA breakage. Since H_2O_2-induced damage is dependent on Fe^{2+}-catalysed hydroxyl radical production (Fenton chemistry), we determined the iron chelation activity of the two test compounds and found that ciclopirox and, to a lesser extent, apomorphine act as iron chelators. We also show that the Fe^{2+} chelation and indirect PARP inhibitory effects of ciclopirox translate to anti-inflammatory actions as demonstrated in a mouse dermatitis model, where ciclopirox reduced ear swelling, inflammatory cell recruitment and poly(ADP-ribosyl)ation.

Conclusion and Implications: Our findings indicate that the antimycotic drug, ciclopirox, acts as an iron chelator and thus targets an early event in hydrogen-peroxide-induced parthanatos. Ciclopirox has the potential to be repurposed as a cytoprotective and anti-inflammatory agent.

Abbreviations: PAR, poly(ADP-ribose); PARG, poly(ADP-ribose) glycohydrolase; PARylation, poly(ADP-ribosyl)ation; PI, propidium iodide.

KEYWORDS
cell death, cytoprotection, inflammation, oxidative stress, PARP1, regulated necrosis

1 | INTRODUCTION

A carefully controlled balance between the production and elimination of reactive oxygen species (ROS) and reactive nitrogen species is of crucial importance for the maintenance of tissue homeostasis. Several reactive oxygen and reactive nitrogen species e.g. **hydrogen peroxide (H_2O_2)** and **nitric oxide (NO)** act as signalling molecules (Droge, 2002). However, in severe pathological conditions (e.g. in stroke, myocardial infarction, pancreatitis and various forms of shock), the production of large amounts of reactive oxygen and reactive nitrogen species contributes to tissue injury. As part of this process, reactive oxygen species (e.g. hydroxyl radical) and reactive nitrogen species (e.g. peroxynitrite) cause cell dysfunction and cell death (Borbely et al., 2005; Lipinski, 2011; Virag et al., 2003). Reactive oxygen/reactive nitrogen species-induced cell injury is triggered by destruction (oxidation) of vital biomolecules (proteins, lipids and DNA). In addition, distinct cell death signalling cascades are initiated by reactive species (Virag et al., 2013). As for the latter, caspase-mediated apoptosis is the "default" cell death pathway in most pathological conditions. However, severe oxidative stress or incapacitation of apoptotic signalling pathways may lead to caspase-independent necrotic pathways (Vanden Berghe et al., 2014; Virag et al., 2013). The major difference between apoptosis and necrosis is that plasma membrane integrity is preserved during apoptosis, whereas plasma membrane permeabilization occurs early during necrosis (Majno & Joris, 1995). Consequent leakage of cellular content from necrotic cells makes necrosis an inflammatory cell death mechanism (Majno & Joris, 1995). Whereas originally necrosis has been regarded as a passive mode of cell death, the last decade brought a paradigm shift demonstrating that various regulated forms of necrosis exist (Robinson et al., 2019; Vanden Berghe et al., 2014). Notable examples of regulated necrosis include necroptosis, pyroptosis, ferroptosis and parthanatos (Robinson et al., 2019).

Parthanatos is a novel form of regulated necrosis mediated by the nuclear DNA nick sensor enzyme **poly(ADP-ribose) polymerase 1 (PARP1)** (Andrabi et al., 2008; Virag et al., 2013). Interestingly, the necrotic and regulated nature of PARP1-dependent cell death has been described way before the terms "regulated necrosis" and "parthanatos" were coined (Virag, Salzman, & Szabo, 1998; Virag, Scott, et al., 1998). These early findings proved that necrosis can be regulated and is therefore amenable to targeted pharmacological interventions (Virag & Szabo, 2002). The canonical form of parthanatos has been characterized in most detail in neuronal excitotoxicity (Andrabi et al., 2008; Yu et al., 2002). In a typical scenario, the excitatory amino acid, **glutamate**, binds to **NMDA receptors** triggering the activation of **neuronal NOS** and production of superoxide. Neuronal NOS-derived NO combines with superoxide to form the potent oxidant species peroxynitrite ($ONOO^-$), which causes DNA breakage (Andrabi et al., 2008; Dawson & Dawson, 2018). PARP1, which binds to and becomes activated by DNA breaks, cleaves its substrate NAD^+ to nicotinamide and ADP-ribose. From the latter cleavage product, PARP1 forms a protein-bound polymer (poly(ADP-ribose) [PAR]) that facilitates the recruitment of DNA repair effector enzymes (Rack et al., 2020). Poly(ADP-ribose) glycohydrolase (PARG) cleaves the polymer off of substrate proteins and PAR moves from the nucleus to the mitochondria, where it triggers the release of apoptosis-inducing factor (Andrabi et al., 2008). Nuclear translocation of apoptosis-inducing factor activates a novel DNA-se enzyme, known as **macrophage migration inhibitory factor (MMFI)**. The activation of MMIF makes the process irreversible (Wang et al., 2016). The key features of this cell death pathway have been confirmed in other cell death models (Greenwald & Pierce, 2019; Kers et al., 2016). However, non-canonical forms of parthanatos that are dependent on PARP1 activation but lack other molecular markers (e.g. apoptosis-inducing factor translocation) have also been reported (Douglas & Baines, 2014; Jang et al., 2017; Regdon et al., 2019).

Oxidative stress-induced DNA breakage, as well as the consequent PARP activation, has been extensively demonstrated in various forms of ischaemia–reperfusion injury, shock and inflammation. Moreover, pharmacological inhibition of PARP1 or genetic

What is already known

- Oxidative stress induces PARP1-mediated cell death termed parthanatos.
- PARP1 mediates many forms of inflammation and tissue injury.

What this study adds

- The antifungal ciclopirox and dopamine agonist apomorphine inhibit parthanatos by acting as iron chelators.
- Ciclopirox exerts anti-inflammatory action in a murine model of dermatitis.

What is the clinical significance

- Ciclopirox could be repurposed for the treatment of oxidative stress-related pathologies.

inactivation of the PARP1 gene has been shown to protect cells from these oxidative stress-related pathologies. These protective effects are linked to the suppression of cell death (parthanatos) and inflammatory signalling, with special regard to the **NF-κB** activation pathway. As for the latter, auto modified PARP1 acts as a co-activator for the inflammatory transcription factor, NF-κB, (Nakajima et al., 2004) explaining the anti-inflammatory effects of PARP inhibitors. In the last few years, PARP inhibitors have entered the clinic as novel anticancer agents, targeting the vulnerability of BRCA1/2-deficient tumours (Curtin, 2014). Based on a vast array of preclinical data (cell-based and animal studies), PARP inhibitors may be suitable for repurposing to treat oxidative stress-related pathologies (e.g. stroke, myocardial infarction, various forms of shock and inflammation) (Berger et al., 2018). Encouraged by the cytoprotective and anti-inflammatory effects of PARP inhibition, we set out to identify novel compounds that inhibit hydrogen-peroxide-induced parthanatos hoping that this effect will translate into anti-inflammatory action. Our high-content screening identified several cytoprotective molecules in a parthanatos model. Two of the hit compounds, ciclopirox and **apomorphine**, appeared especially interesting, as they act proximal to PARP1 activation, while the others act distally. Ciclopirox also showed anti-inflammatory effects, proving the success of our strategy to target a pathway that is active in both cell death and inflammation.

2 | METHODS

2.1 | Materials

RPMI-1640 medium (SLM-140), FBS, MTT (M2003-1G), propidium iodide (PI) (P4864-10ML), and phorbol 12-myristate 13-acetate (PMA; reactive oxygen species) were purchased from Sigma-Aldrich (Budapest, Hungary). PJ34 (2-(dimethylamino)-*N*-(6-oxo-5*H*-phenanthridin-2-yl)acetamide hydrochloride) was obtained from ??. Penicillin–streptomycin and L-glutamine were from Lonza (Basel, Switzerland). DAPI (D1306), Hoechst 33342 (H3570) and Sytox Green (S7020) were purchased from Invitrogen (Carlsbad, CA, USA). The anti-PARP1 antibody (46D11; rabbit mAb #9532) (RRID:AB_659884) was purchased from Cell Signaling Technology (Danvers, MA, USA). The anti-PAR antibody was purified from the culture medium of the 10H hybridoma clone. The anti-phospho-H2AX antibody (4418-APC-020) was purchased from Trevigen (Minneapolis, MN, USA). The compound library was Screen-Well® FDA Approved Drug Library V2 (BML-2843-0100, Enzo Life Sciences, Farmingdale, NY, USA).

2.2 | Cell culture

HaCat (RRID:CVCL_0038) cells were cultured in RPMI supplemented with 10% FBS, 1% L-glutamine and penicillin/streptomycin solution (50 U·ml^{-1} and 50 μg·ml^{-1}, respectively).

2.3 | High-content analysis of H_2O_2-induced cytotoxicity for the identification of cytoprotective compounds

HaCat cells were seeded into CellCarrier Ultra 96-well microplates (Perkin Elmer) at a seeding density of 3,000 cells per well and a final volume of 75 μl. The plates were incubated in normal cell culturing conditions overnight. Compounds of the library were transferred to the plates with a Tecan Freedom EVO liquid handling robot to reach 20-μM final concentration. Cells were incubated for 60 min and cytotoxicity was induced with 75 μl of H_2O_2 solution. The final concentrations of the compounds were 10 μM and the H_2O_2 was 200 μM. Cells were incubated for an additional 8 h followed by Sytox Green staining as follows. Cells were stained with Sytox Green (200 nM) and Hoechst (5 μg·ml^{-1}) for 10 min. Images were taken with an Opera Phenix high-content screening system (Perkin Elmer) using 10X air objective and appropriate laser and filter settings in sequential mode to avoid overlapping of the emission spectra. Images were analysed with the Harmony software (Perkin Elmer). First, images were segmented based on Hoechst staining using the "Find nuclei" software module (channel: Hoechst, method: M, diameter: 20 μm, splitting sensitivity: 0.30, common threshold: 0.30). Nuclear morphology parameters were calculated (method: standard [area, roundness, width, length, ratio width to length] and method: STAR). After removing the border objects, improperly defined nuclei were removed using built-in machine learning protocols (PhenoLOGIC) based on the morphology parameters calculated previously using the "Select population" building block (method: linear classifier, number of classes: 2). Remaining nuclei were defined as "true nuclei" and used for further analysis. To increase signal-to-noise ratio, the background was subtracted with "Filter image" building block (channel: Sytox Green, method: Sliding parabola). The mean fluorescence intensity of Sytox Green was calculated (calculate intensity properties: channel: Sytox Green [Sliding parabola], method: standard [mean]) and a new "necrotic" population was introduced with the "Select population" building block (method: filter by property, parameter: Sytox Green mean intensity > 200, output population: necrotic). Necrosis % was calculated in the "Define results" building block with the following formula: necrotic (number of objects)/true nuclei (number of objects) × 100. Compounds that had higher than 50% cytoprotective effects were considered hits.

2.4 | MTT assay for cell viability

Cell viability was measured with MTT assay. MTT solution (0.5 mg·ml^{-1}) was added to plates and cells were incubated for 60 min. The medium was aspirated and formazan crystals were dissolved in 100-μl DMSO. Absorbance was measured at 590 nm on a Tecan Spark plate reader (Tecan). Viability was calculated and expressed as the per cent of control.

2.5 | Analysis of thymocyte death by flow cytometry

Thymocyte isolation was carried out as described (Hegedus et al., 2008). C57/Bl6 mice (4–6 week old) were killed with isoflurane and the thymi were aseptically dissected, placed into ice-cold RPMI 1640 medium (10% fetal calf serum, 10-mM L-glutamine, 100 U·ml^{-1} penicillin and 10 μg·ml^{-1} streptomycin) and sieved through a stainless steel wire mesh and a 100-μm nylon filter to prepare single-cell suspensions. The thymocytes were diluted to 2 × 10^6/ml density with medium and seeded into 96-well plates per 100 μl. Next, ciclopirox or apomorphine was added to the wells to the required concentrations for 30 min, after which 200-μM H_2O_2 was added where necessary. Following a 4.5-h incubation, the cells were stained with 1.25 μg·μl^{-1} PI for 5 min and cell death was measured with an Acea NovoCyte flow cytometer.

2.6 | Immunofluorescent staining and fluorescent microscopy

HaCat cells were seeded into CellCarrier Ultra plates (Perkin Elmer). Cells were treated as indicated in figure legends, then washed with PBS and fixed with methanol for 20 min at −20°C for PAR polymer (10H clone) and PARP1 or fixed in 4% PFA at room temperature for 15 min for γH_2AX staining. Cells were then washed three times with PBS, permeabilized with 0.5% Triton-X in PBS for 5 min and blocked with 1% BSA in PBS for 60 min. Cells were incubated with primary antibodies in blocking solution overnight at 4°C with gentle agitation. After washing three times with PBS, cells were incubated with the secondary antibody (1:1,000 dilution) and DAPI (2 μg·ml^{-1}) in PBS for 45 min. Cells were washed three times with PBS and were kept in PBS until fluorescence microscopy. Imaging was carried out with an Opera Phenix High-Content Analysis System (Perkin Elmer). Staining and image acquisition conditions are specified in figure legends. All image analysis was performed with the Harmony software (Perkin Elmer).

2.7 | Measurement of H_2O_2 and mitochondrial superoxide production

After incubation with H_2O_2, HaCat cells were washed three times with PBS and incubated for 30 min with 2.5-μM H_2DCFDA (for H_2O_2 assay) or 5-μM MitoSOX Red (for superoxide assay) (Kovacs et al., 2012). Cells were washed three times with PBS again and fluorescence intensity was measured at 494/538 nm (H_2O_2) or 510/598 nm (superoxide) with a Tecan Spark fluorescent plate reader (Tecan, Männedorf, Switzerland). Control experiments showed that no residual H_2O_2 remained in the wells after our extensive washing protocol.

2.8 | Transfection

The PARP1-mCherry OmicsLink expression plasmid was acquired from GeneCopoeia. HaCat cells were plated into Ibidi eight-well μ chamber slides the previous day. Two hours before transfection, the cells were treated with the K4 Multiplier reagent of the K4 Transfection System (Biontex) diluted 100-fold in the culture medium. Plasmid DNA (300 ng per well) mixed with Lipofectamine 3000 at a 1:1 μg to μl ratio was added to wells in Opti-MEM. The medium was changed 5 h later to normal culture medium containing 1/200 K4 Multiplier. The cells were used for microirradiation 36–48 h later.

2.9 | Microirradiation and image analysis

Laser microirradiation was performed with a Leica TCS SP8 confocal microscope using the FRAP module of the LAS X software. The cells sitting in Ibidi eight-well chamber slides with a coverslip bottom were pretreated with ciclopirox or apomorphine together with 10 μg·ml^{-1} Hoechst 33342 for 30 min after which the medium was changed to FluoroBright containing the investigated compounds but no Hoechst. Images were acquired with a Leica HC PL Apo CS 40×/NA 0.85 dry objective through a 99.94-μm-diameter pinhole (1 Airy unit) resulting in an optical slice thickness of 1.6 μm. The zoom factor was set to 2× and frames were acquired with 400-Hz bidirectional scanning at 1,024 × 256-px digital resolution. A 552-nm OPSL laser was used to excite mCherry. For the microirradiation of the PARP1-mCherry-transfected cells, the 0.4-mW 405-nm diode laser was tuned to 3.5% power and was parked over a point in the nucleus for 2 ms using LAS X's PointBleach function. Forty pre-irradiation images were collected every 328 ms. Following laser microirradiation, 200 images were taken with the settings used during the pre-irradiation period and a further 230 every second. The intensity of the region of protein recruitment at a given time (I_t) was measured with ImageJ (RRID: SCR_003070) after the images had been registered using the StackReg plugin, using rigid body transformation. Bleaching due to image acquisition was insignificant based on the lack of change in intensity during the pre-irradiation period. The average pre-irradiation intensity was subtracted from I_t and the increase of intensity was normalized to the highest value of the average of the sample during the post-irradiation period.

2.10 | Comet assay

The Alkaline Comet assay was performed using Trevigen Flare slides, according to the manufacturer's instructions and a previously published paper (Kovacs et al., 2012) with some modifications as follows. After trypsinization, 10^5 cells were pretreated with DMSO (vehicle), apomorphine (10 μM) or ciclopirox (10 μM) for 1 h. H_2O_2 was added at a final concentration of 200 μM for 10 min. Then

cells were centrifuged at 4°C and resuspended in 1-ml ice-cold PBS. The cell suspension (40 μl) was combined with 400-μl molten LM agarose (1%, 37°C) and 40 μl of this mixture was immediately pipetted onto a FLARE slide. Slides were placed at 4°C in the dark for 30 min and then immersed in cold Lysis Solution (Trevigen). After overnight lysis, slides were immersed in electrophoresis buffer (0.03-M NaOH, 2-mM Na_2EDTA, pH ~ 12.3) at room temperature for 3 × 30 min to equilibrate the slides. Electrophoresis was conducted at 4°C for 30 min at 20 V. After rinsing and neutralizing in distilled water, nuclei were stained with 10 $\mu g \cdot ml^{-1}$ PI solution for 30 min. After washing with distilled water, slides were dried at room temperature to bring the cells to the same plane. Before analysis, a thin layer of molten 1% LM agarose was added onto the slides to reduce background fluorescence. Images were taken by Leica SP8 Confocal Microscope. Comets were analysed with Open Comet software. Cells (n = 50) were randomly selected from all conditions in each experiment for the statistical analysis.

2.11 | PARP1 chromatin binding assay (PARP1 trapping assay)

HaCat cells were seeded into CellCarrier Ultra plates (Perkin Elmer). Cells were treated as indicated in figure legends. Then cells were pre-extracted on ice in 0.2% Triton X-100 for 2 min, fixed with methanol at −20°C and stained for PARP1, as described above (Michelena et al., 2018).

2.12 | Calcein dequenching assay (detection of intracellular iron chelation)

HaCat cells were seeded into 96-well plates at a density of 20,000 cells per well the day before the experiment. Then the cells were incubated with 250-nM calcein-AM in normal culture medium (RPMI 1640, 10% fetal calf serum, 10-mM L-glutamine, 100 $U \cdot ml^{-1}$ penicillin, 10 $\mu g \cdot ml^{-1}$ streptomycin) for an hour. Cells were washed two times with HBSS containing 0.4-mM calcium and magnesium and incubated for 30 min to allow the uncleaved calcein-AM to diffuse out of the cells. The medium was changed to HBSS containing 2.5 $\mu g \cdot ml^{-1}$ propidium iodide (PI) and the cells were incubated for another 30 min to allow PI to equilibrate between the medium and the cell interior. The plates were placed into a Spark multimode plate reader (Tecan Life Sciences) and both the calcein and the PI fluorescence were recorded kinetically. The recording consisted of three phases. After an initial equilibration period of 15 min, 10-μM CPX or APO was injected into the designated wells with the instrument's injector pump and the dequenching of calcein fluorescence was followed for 30 min. Finally, a third phase, in which 200-μM H_2O_2 was injected into the designated wells and its effect on the intracellular labile iron pool was observed as a change in the calcein fluorescence for 45 min.

2.13 | Dermatitis model

Animal experiments were approved by the institutional animal welfare committee (protocol 15/2016/DEMÁB). Animal studies are reported in compliance with the ARRIVE guidelines (Percie du Sert et al., 2020) and with the recommendations made by the *British Journal of Pharmacology* (Lilley et al., 2020). The dermatitis model was carried out as previously described (Bakondi et al., 2019) with modifications as follows. BALB/c mice (18 males and 18 females) were used at 10–12 weeks of age. Mice were housed in Euro-standard Type II cages under standard temperature, humidity and light-controlled conditions (21–23°C, 30–60% relative humidity, 12-h light/dark cycles) and were fed *ad libitum*. Dermatitis was induced with **phorbol 12-myristate 13-acetate (PMA)**. Animals were randomized into three groups. The control group was treated with vehicle (DMSO). The PMA group was treated with 0.05% PMA and the PMA-ciclopirox group with 0.05% PMA and 1 m/V % ciclopirox (in DMSO). Before the induction of inflammation, the ear thickness of mice was measured with a Mitutoyo thickness gauge. Mice were then treated with DMSO or PMA (20 μl per ear applied with a micropipette, 10 μl to each side of the ear). Sixty minutes later, the control and PMA groups were treated with DMSO and the PMA-ciclopirox group was treated with 10-μM ciclopirox (20 μl smeared onto the ears with a micropipette, 10 μl to each side of the ear). Six hours after the PMA treatment, the ear thickness was measured again and mice were killed with isoflurane. The ears of the animals were removed for histology (standard haematoxylin–eosin staining), immunohistochemistry for PAR polymer and myeloperoxidase activity assays (see below).

2.14 | Immunohistochemistry

PAR polymer was detected by immunohistochemistry, as described by Gehl et al. (2012). Briefly, 5-μm sections were cut from paraffin-embedded ear tissues. After deparaffinization, endogenous peroxidase activity was blocked in 3% (v/v) H_2O_2 solution (20 min). Sections were rinsed in PBS and antigen retrieval was carried out by incubating sections at 100°C in 0.01-M sodium citrate buffer (pH 6.0). Sections were rinsed in dH_2O and washed in PBS for 5 min. Blocking was carried out in PBS containing 1% (w/v) BSA and 1% (v/v) horse serum for 60 min. Mouse monoclonal PAR-specific antibody (purified in house from clone 10H hybridoma supernatant; isotype IgG3) was applied at 3 $\mu g \cdot ml^{-1}$ concentration in the blocking solution overnight at 4°C. After 3 × 10-min washes in PBS, secondary antibody (biotin-conjugated horse anti-mouse IgG; supplied in a Vectastain kit; Vector Laboratories, Burlingame, CA, USA) was diluted 600× in the blocking solution and applied for 45 min at room temperature. After 3 × 10-min washes in PBS, sections were treated for 30 min with 2% avidin–biotin–peroxidase reagent (supplied in the Vectastain kit). After 3 × 10-min washes in PBS, colour was developed with Ni-DAB substrate (1.6-mM 3,3-diaminobenzidine, 140-mM NaCl, 90-mM $NiSO_4$, 100-mM Na-acetate, 3-mM H_2O_2, pH 6.6). Sections were

rinsed in 0.5% cobalt chloride (dissolved in 0.1-M Tris-buffered saline, pH 7.2), After rinsing sections in dH_2O, counterstaining was performed with 0.005% (v/v in acetic acid) Chromotrop 2R (Chroma, Stuttgart, Germany). Stained images were semiquantitatively evaluated by a trained pathologist who was blinded to the experimental design and identity of samples. The scoring scheme ranging from 0 to 3 was used as follows:- 0 negative (no or negligible amount of PAR signal); 1 weak (scattered PAR positivity); 2 moderate (PAR signal is detectable in 20–30% of cells) and 3 strong (PAR signal in the majority of cells). The Immuno-related procedures used comply with the recommendations made by the *British Journal of Pharmacology* (Alexander et al., 2018).

2.15 | Myeloperoxidase activity

Myeloperoxidase activity has been determined as described (Brunyanszki et al., 2010). Tissue samples were weighed, thawed and homogenized in 1 ml of 20-mM phosphate buffer (pH 7.4) and then centrifuged at 13,000 rpm for 30 min at 4°C. The resulting pellet was resuspended in 0.5 ml of 50 mmol·L^{-1} phosphate buffer (pH 6.0) containing 0.5% HTAB (Sigma). The homogenates were then frozen in liquid nitrogen and thawed in three consecutive cycles before sonication. The samples were then centrifuged (13,000 rpm for 30 min at 4°C) and the supernatants were collected for the myeloperoxidase assay. The supernatant (100 μl) was mixed with 100-μl solution of 1.6-mM 3,3′,5,5′-tetramethylbenzidine (Sigma-Aldrich) and 1-mM hydrogen peroxide. The mixture was incubated at 37°C for 120 s and the reaction was stopped with 200-μl 2-M H_2SO_4. The absorbance was measured at 450 nm and then normalized to tissue weight.

2.16 | Data and analysis

The data and statistical analysis comply with the recommendations of the *British Journal of Pharmacology* on experimental design and analysis in pharmacology (Curtis et al., 2018). All experiments on cell lines were designed with groups of equal sizes in a blinded and randomized manner. Shapiro–Wilk test was used for normality testing. Data are presented as mean and SD from Gaussian data or median and interquartile range (violin plot) from non-Gaussian data. Samples from non-Gaussian data were tested with Mann–Whitney *U* test or Kruskal–Wallis test where two or more groups were analysed respectively. Samples from Gaussian data were tested for equal variance and the appropriate unpaired Welch's *t*-test or one-way/two-way ANOVA was used for calculating statistical significance. Post hoc tests were used if *F* was significant (in ANOVA analyses). Discrete data were analysed by Fisher's exact test. For animal experiments, the group size estimation was designed to be equal considering 80% power with G Power software (version 3.1.9.4) and to avoid using an unnecessary number of animals (3R principles). *P* values less than 0.05 were considered significant. Data analyses were performed with GraphPad Prism (version 8.0.1) (RRID:SCR_002798) software. Statistical analysis was undertaken only for studies where each group size was at least $n = 5$. This requirement was met by all experiments presented in this paper except the compound library screen. The declared group size is the number of independent values and statistical analysis was done using these independent values and not technical replicates. Data were normalized to control in the cases where it was necessary because of technical aspects of the assay (Figures 2c, 3a,b and 7). Outliers were included in data analysis and presentation with one exemption as follows. In experiments presented in Figure 5a,b, outliers were excluded because in this experiment, a total of 1,000 cells were analysed (5*200) and excessively high values would change the mean of the population to a large extent. Outliers were excluded with GraphPad Prism 8 using the "find outliers" option to remove definitive outliers ($Q = 0.5\%$). Cleaned data were presented and analysed.

2.17 | Nomenclature of targets and ligands

Key protein targets and ligands in this article are hyperlinked to corresponding entries in the IUPHAR/BPS Guide to PHARMACOLOGY http://www.guidetopharmacology.org and are permanently archived in the Concise Guide to PHARMACOLOGY 2019/20 (Alexander et al., 2019a,b).

3 | RESULTS

3.1 | Setting up a high-content analysis-compatible assay for the detection of PARP1-dependent cell death (parthanatos)

To identify novel molecular tools targeting parthanatos, we developed a high-content analysis assay for the determination of hydrogen-peroxide-induced cell death. Since oxidative stress-induced PARP1 activation has previously been demonstrated in HaCat keratinocyte cells *in vitro* (Bakondi et al., 2003, 2004; Szabo et al., 2001) and in skin inflammation *in vivo* (Szabo et al., 2001), we chose HaCat cells for our study. After optimization of assay conditions (Figure S1), the following optimal conditions were selected for the screening. Cells were pretreated at a 10-μM concentration for 1 h with library compounds. Hydrogen-peroxide-induced (200 μM) cell death was measured at the 8-h time point (Figure S1B). The cell death assay is based on the detection of plasma membrane permeabilization using the cell impermeable fluorescent dye, Sytox Green. Nuclei were stained with Hoechst dye and the Hoechst channel was used to identify nuclei as regions of interest (ROI). The intensity of Sytox Green fluorescence was determined in the nuclear area (Figure S1C). Using various H_2O_2 concentrations and treatment times, we determined cell death in the presence or absence of the PARP inhibitor PJ34 (positive control) (Jagtap et al., 2002) and selected optimal conditions for assaying PARP1-mediated cell death (Figure S1D).

3.2 | Compound library screening and identification of molecules protecting cells from parthanatos

After setting up the above high-content screening compatible assay, we determined the suitability of the assay for high-content screening. Using a small library of 774 FDA (US Food and Drug Administration) approved compounds, we performed a screen. Every screening plate contained four untreated wells (CTL), eight hydrogen-peroxide-treated wells and four PJ34 + H_2O_2-treated wells to detect PARP1-dependent necrosis. The mean necrosis (%) values plotted with the corresponding SD values indicate clear discrimination of the three groups (CTL, H_2O_2 and PJ34 + H_2O_2) (Figure 1a). To confirm the robustness of the assay, the *Z* factor was calculated for all 10 screening plates. The assay displayed outstanding discriminating power (Figure 1b). *Z* factor is a screening window coefficient reflective of both the assay signal dynamic range and the data variation associated with the signal measurements. A *Z* factor between 0.5 and 1.0 is considered an excellent assay (Zhang et al., 1999). In our screen, all plates had a $Z' > 0.5$. After making sure that our screen was reliable, we pooled our screening data from all 10 test plates (Figure 1c). To eliminate interplate variance, the pooled data were plotted as per cent cytoprotection values on a dot plot (Figure 1c). A 50% cytoprotection threshold was set and molecules above the threshold ($n = 20$) were considered hits.

3.3 | Validation of selected cytoprotective hits

The 20 hit compounds (Table 1) were scrutinized to determine which hits had potentially novel and relevant cytoprotective effects. Antineoplastic agents, including idarubicin, doxorubicin, mitoxantrone, dactinomycin and epirubicin, were excluded. Manual re-evaluation of primary images showed that four hits caused false positives due to assay interference. These drugs are DNA intercalating agents that prevent DNA intercalation of the Sytox Green dye (Table 1). Eventually, we selected seven hit compounds for verification. In confirmatory assays, all seven had significant cytoprotective effects; ciclopirox, rifaximin and apomorphine were most potent (Figure 2).

3.4 | Characterization of the cytoprotective effects of ciclopirox and apomorphine

To provide additional evidence for the cytoprotective effects of ciclopirox and apomorphine, we determined their IC_{50} values with the same cell type (HaCat cells) but with a different assay (MTT). In MTT assays on H_2O_2-treated HaCat cells, ciclopirox and apomorphine had IC_{50} values of 2.4 and 9.3 μM, respectively (Figure 3a).

We also sought to investigate whether the cytoprotective effects of ciclopirox and apomorphine were cell type specific. We chose thymocytes, a non-adherent primary cell type, for this confirmatory experiment. We chose thymocytes because the PARP1-mediated necrotic cell death pathway has been well characterized in this model. In fact, the necrotic feature and mitochondrial dysfunction in PARP1-mediated cell death were first demonstrated in this cell type (Virag, Salzman, & Szabo, 1998; Virag, Scott, et al., 1998). We found that both ciclopirox and apomorphine markedly protected thymocytes from H_2O_2-induced necrotic cell death

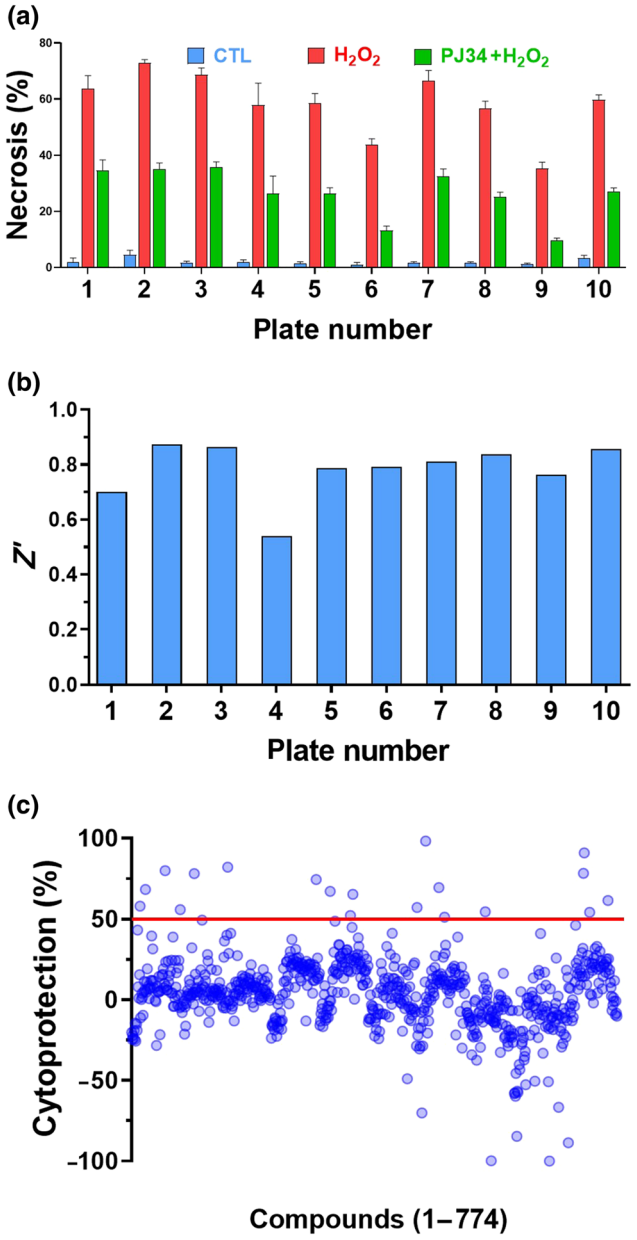

FIGURE 1 Screening results. (a) Every screening plate contained four untreated wells (CTL), eight H_2O_2-treated wells and four PJ34 + H_2O_2-treated wells to detect PARP-dependent necrosis. Necrosis (%) mean and SD are presented. (b) *Z* factor was calculated to characterize assay robustness for each plate. Four negative controls and eight positive controls were used. (c) Pooled data containing all compounds are presented as cytoprotection (%) instead of necrosis (%) to eliminate interplate variance. Drugs showing cytoprotection > 50% were considered "hits"

TABLE 1 Cytoprotective hit compounds identified in the high-content screening

Cluster	Compound name	Cytoprotection (%)	Usage	Mechanism of action
Adrenergic receptor signalling	Phentolamine	57.99	Vasodilator	Competitively blocking α-adrenoceptors
	Prazosin	68.31	Antihypertensive	Inhibits the postsynaptic α_1-adrenoceptors on vascular smooth muscle
	Apomorphine	79.98	Non-selective dopamine agonist and anti-Parkinsonian	Dopamine agonist
	Formoterol	54.44	Antiasthmatic, bronchodilator	A long-acting β_2-agonist
Serotinin receptor signalling	Sertraline	54.06	Antidepressant	Selectively inhibits the reuptake of 5-HT (serotonin) at the presynaptic membrane
	Fluoxetine	52.17	Used for the treatment of major depression	Selective 5-HT (serotonin) reuptake inhibitor
Affects intracellular Ca^{2+} level	Nisoldipine	55.79	Antihypertensive, vasodilator	Calcium channel blocker of the dihydropyridine class
	Amrinone	65.33	Increases the contractions initiated in the heart and can be used with patients that have congestive heart failure	PDE inhibitor (PDE3)
Chelator (Fe)	Deferasirox	51.17	Rationally designed iron chelator	Used to reduce chronic iron overload
DNA binding, transcription inhibition	Actinomycin D	69.45	Antineoplastic	Inhibits transcription by binding DNA at the transcription initiation complex and preventing elongation by RNA polymerase
	Rifapentine	78.24	Antibiotic, antitubercular	Inhibits DNA-dependent RNA polymerase in susceptible strains of *M. tuberculosis*
	Rifaximin	90.88	Anti-infective, gastrointestinal agent	Acts by inhibiting RNA synthesis in susceptible bacteria by binding to the β-subunit of bacterial DNA-dependent RNA polymerase enzyme
	Primaquine diphosphate	67.13	Antimalarial, antiprotozoal	It may be acting by generating ROS or by interfering with the electron transport in the parasite. Also, although its mechanism of action is unclear, primaquine may bind to and alter the properties of protozoal DNA
Inhibit translation	Tigecycline	61.43	Antibiotic	Inhibits protein translation in bacteria by binding to the 30S ribosomal subunit and blocking entry of amino-acyl tRNA molecules into the A site of the ribosome
DNA intercalating	Idarubicin	78.03	Antineoplastic, antibiotic	Intercalates between DNA base pairs and also inhibits topoisomerase II by stabilizing the DNA–topoisomerase II complex and inhibiting topoisomerase II catalysed religation
	Doxorubicin	82.05	Antineoplastic	DNA intercalator
	Mitoxantrone	74.46	Antineoplastic	Intercalates between DNA base pairs and also inhibits topoisomerase II
	Epirubicin	100.00	Antineoplastic	Anthracycline-type DNA intercalator, triggers DNA cleavage by

TABLE 1 (Continued)

Cluster	Compound name	Cytoprotection (%)	Usage	Mechanism of action
				topoisomerase II and DNA damage by free radical generation
Bacterial cell wall synthesis inhibitor	Ceftibuten	57.11	Antibiotic	3rd-generation cephalosporin; bacterial cell wall synthesis inhibitor
Unknown	Ciclopirox	98.31	Antifungal	The mechanism of the antifungal effect is unknown. Loss of function of catalase and peroxidase enzymes, interruption of $Na^+ K^+$ ATP-ase, disruption of DNA repair and mitosis have been suggested as possible mechanisms

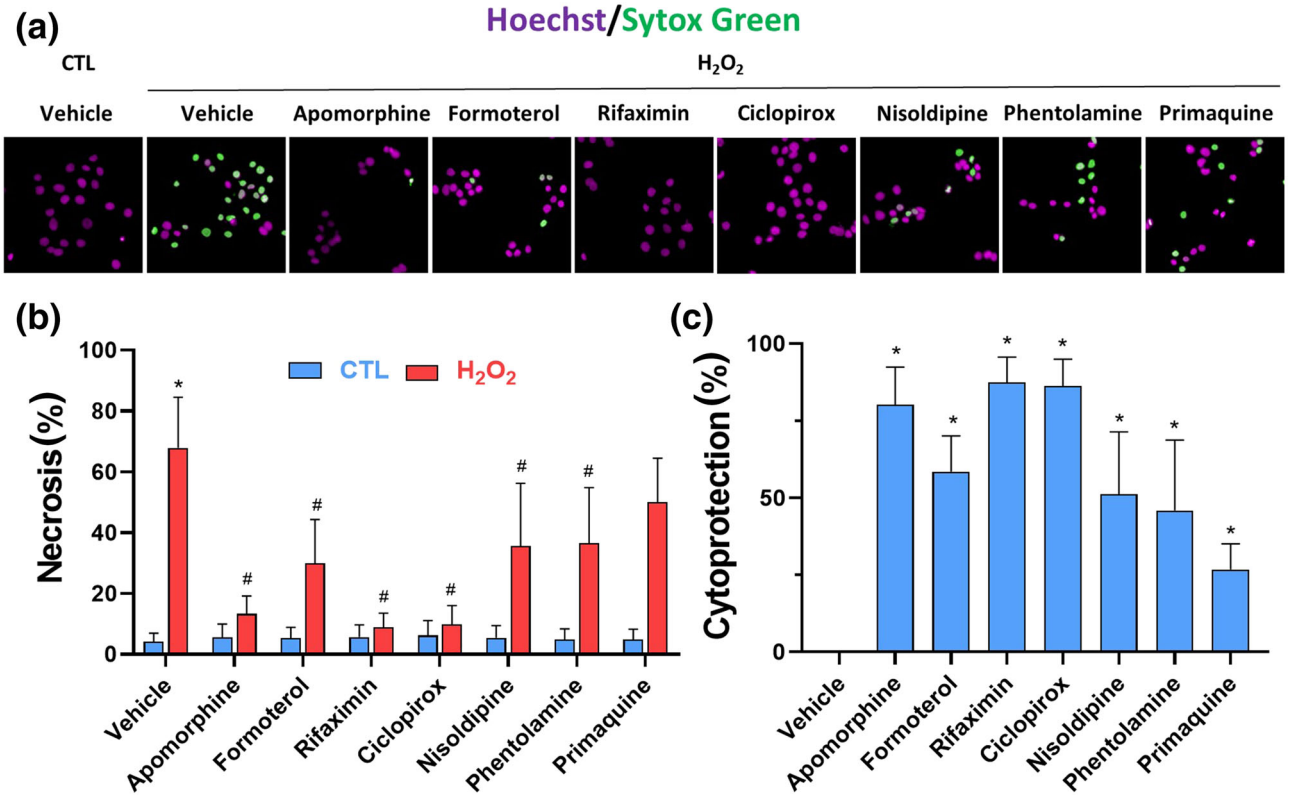

FIGURE 2 Hit validation. HaCat cells were pretreated with 10-μM test compounds for 60 min and cytotoxicity was induced with 200-μM H_2O_2 for 8 h. Necrosis was detected with the Sytox Green assay. (a) Representative images: Hoechst (purple) staining all nuclei and Sytox Green (green) staining necrotic nuclei. (b) Per cent necrosis values are presented as mean and SD. Statistical analysis was performed with one-way ANOVA followed by Dunnett's test. (c) Cytoprotection (%) data are presented as mean and SD. Statistical analysis was performed with one-way ANOVA followed by Dunnett's test

(Figure 3b). The IC_{50} for the cytoprotective effect of ciclopirox was 2.5 μM, whereas apomorphine was more effective in thymocytes (IC_{50} 1.3 μM) (Figure 3b) than in HaCat cells. The difference between IC_{50} values obtained in the HaCat versus thymocyte experiments may be due to differences in drug uptake or oxidative cell death signalling.

Many forms of cell death, including parthanatos, are associated with chromatin condensation (Regdon et al., 2019). Nuclear condensation was observed in H_2O_2-treated HaCat cells and both ciclopirox and apomorphine inhibited this morphological alteration more potently than the PARP inhibitor PJ34 (Figure 3c).

3.5 | Ciclopirox and apomorphine inhibit H_2O_2-induced PARylation

Next, we set out to determine if these seven compounds inhibited H_2O_2-induced PARP activation or act downstream of PARP1 in the

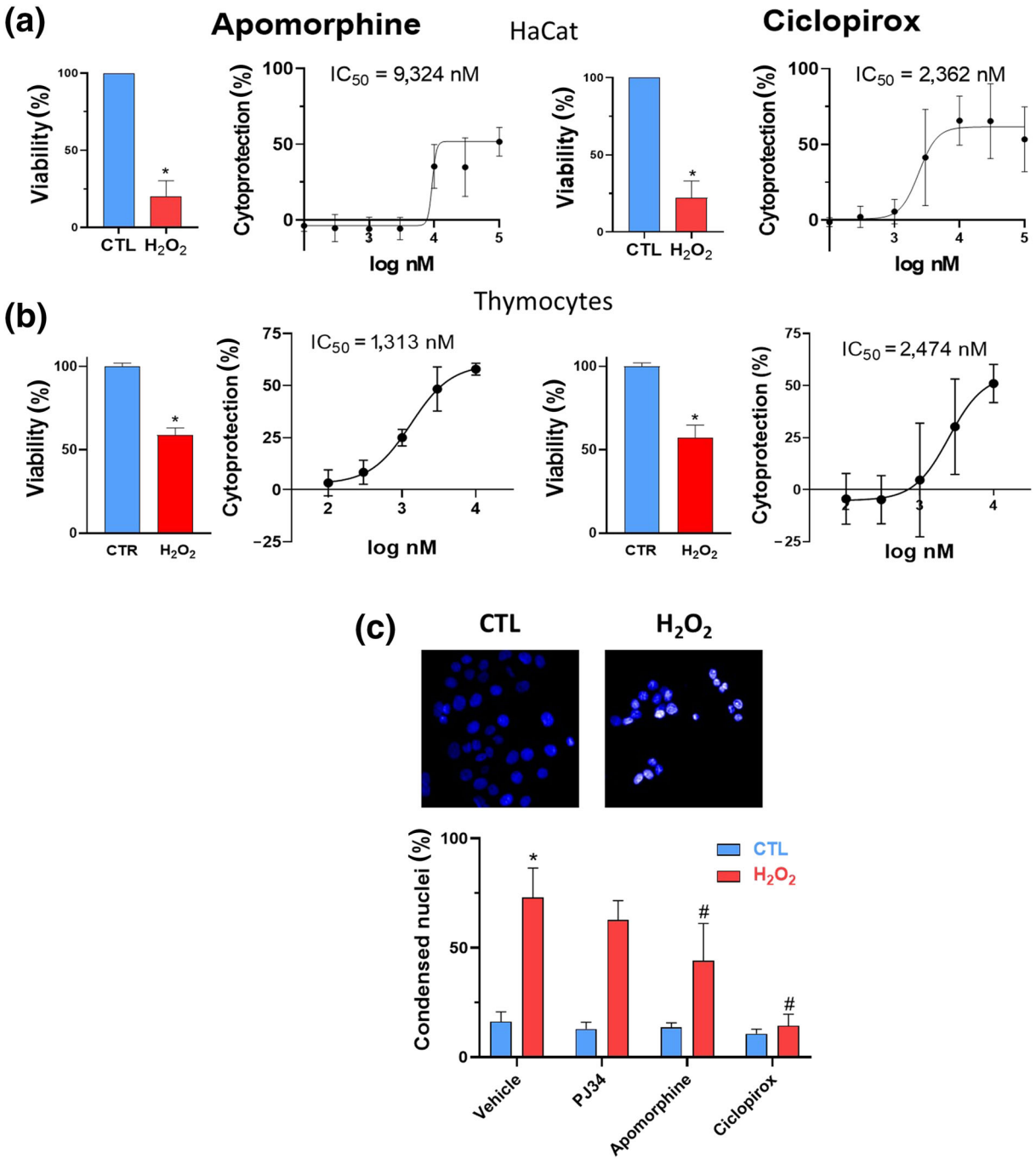

FIGURE 3 Confirmation of the cytoprotective effects of ciclopirox (CIP) and apomorphine (AMO). (a) HaCat cells were pretreated with CIP or AMO at the indicated concentrations for 60 min and then exposed to 200-μM H_2O_2 for 8 h. Viability was measured using an MTT assay. Data are presented as mean and SD. IC_{50} values were calculated from interpolated data. The effects of H_2O_2 were analysed with a Welch's *t*-test. (b) Mouse thymocytes were pretreated with the indicated concentrations of CIP or AMO for 30 min; then 200-μM H_2O_2 was added to the cells for another 4.5 h. Following a 5-min incubation with 1.25 $\mu g \cdot ml^{-1}$ propidium iodide, cell death was measured by flow cytometry. Data are presented as mean and SD. IC_{50} values were calculated from interpolated data. The effect of H_2O_2 was analysed with a Welch's *t* test. (c) HaCat cells were pretreated with the indicated compounds and cell death was induced with 200-μM H_2O_2 for 8 h. Cells were stained with Hoechst and imaged with a fluorescent microscope. Cells were classified as having "normal" or "condensed" nuclei (expressed as a per cent of total nuclei). Mean and SD are presented. Statistical analysis was performed with one-way ANOVA followed by Dunnett's test

cell death pathway. We first determined the dynamics of PAR synthesis and degradation in H_2O_2-treated HaCat cells by immunofluorescent staining for PAR polymers. We found that polymer levels peaked between 5 and 15 min after H_2O_2 exposure (Figure 4a). Thus, we selected the 10-min time point and tested our seven selected hit compounds to see how they affect PAR synthesis. Interestingly, only

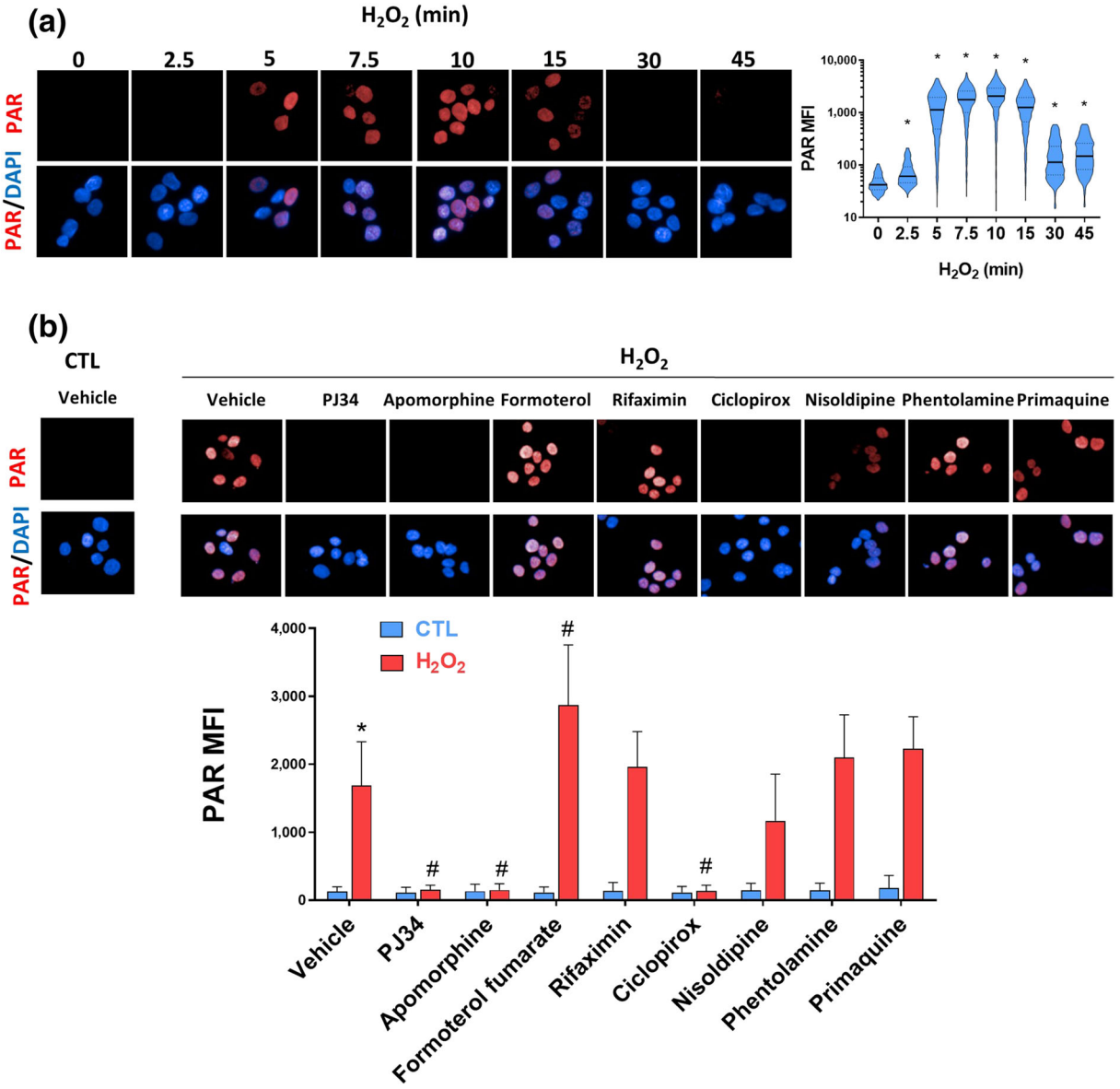

FIGURE 4 Ciclopirox (CIP) and apomorphine (AMO) inhibit PARylation. (a) The time course of PARylation. HaCat cells were treated with 200-μM H_2O_2 for the indicated times. Cells were fixed and stained for PAR. Mean fluorescence intensity was calculated for individual nuclei. The violin plot shows the mean intensity for 1,000 cells per condition. Statistical analysis was performed with Kruskal–Wallis test. (b) HaCat cells were pretreated with test compounds (10 μM), and PARylation was induced with 200-μM H_2O_2 for 10 min. Mean intensity and SD are presented. Statistical analysis was performed with one-way ANOVA followed by Dunnett's test

ciclopirox and apomorphine blocked PAR synthesis. Formoterol slightly increased PAR synthesis, while all other compounds had no effect (Figure 4b). Assuming that interventions targeting early events in cytotoxic signalling may be superior cytoprotective agents, we continued the mechanistic investigation with ciclopirox and apomorphine.

3.6 | Ciclopirox and apomorphine prevent hydrogen-peroxide-induced PARP1 chromatin binding

The next question we wished to answer was whether ciclopirox and apomorphine target PARP1 directly or indirectly target proximal steps of oxidative DNA damage signalling. PARP1 rapidly binds to DNA nicks and detaches from DNA following auto-poly (ADP-ribosyl)ation (PARylation). Some PARP inhibitors, for example, olaparib, trap PARP1 on broken DNA (Murai et al., 2012), whereas others (e.g. PJ34) inhibit PARP1 activity without causing toxic DNA–PARP1 complexes. We demonstrate here that hydrogen peroxide induces increased PARP1 chromatin binding (Figure 5a,b). Both ciclopirox and apomorphine significantly reduced the binding of PARP1 to the chromatin. The PARP1 trapping inhibitor olaparib enhanced hydrogen-peroxide-induced PARP1 chromatin binding whereas the non-trapping inhibitor PJ34 had no effect. iclopirox and apomorphine greatly reduced the trapping effect of olaparib

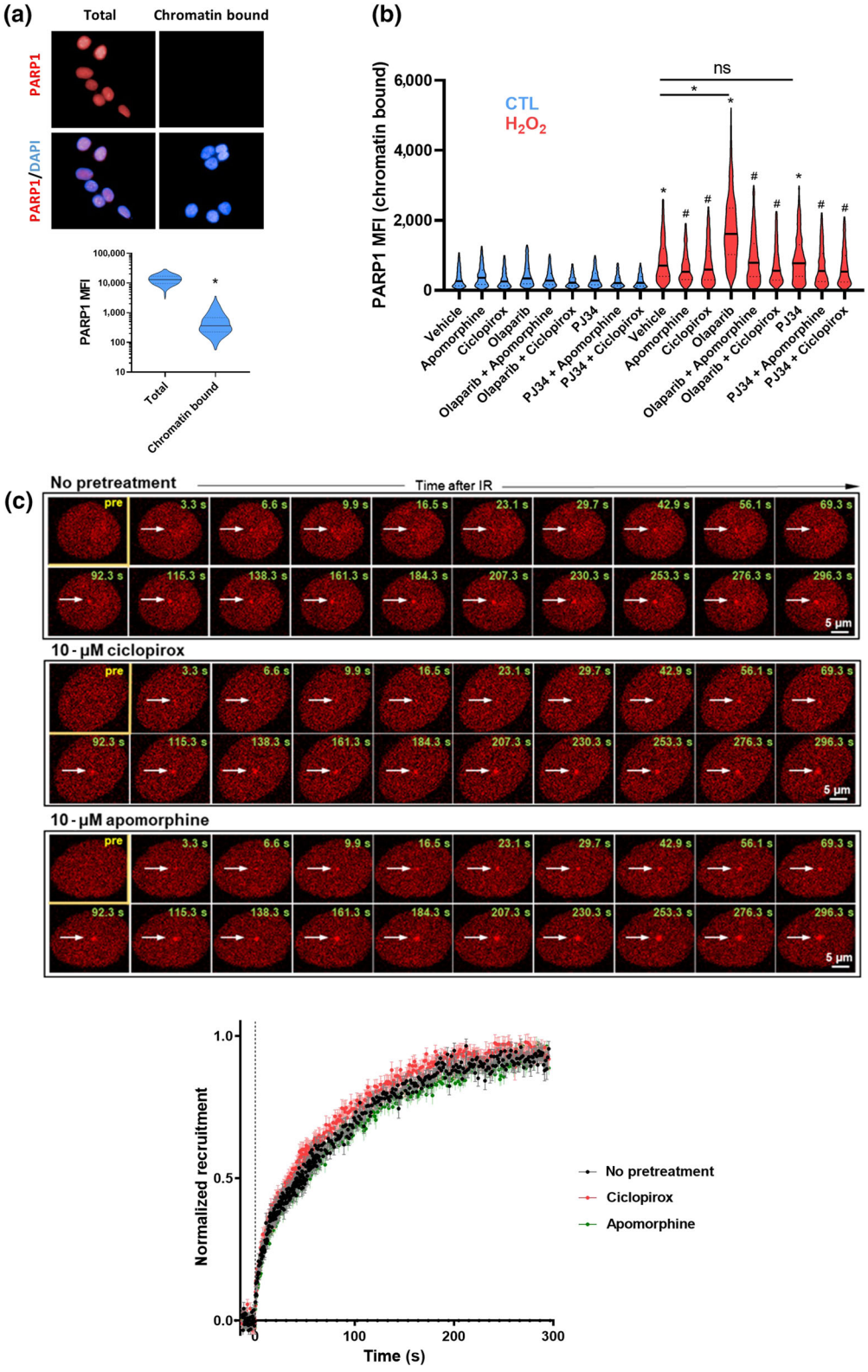

FIGURE 5 Ciclopirox (CIP) and apomorphine (AMO) prevent chromatin binding of PARP1. (a) HaCat cells were left untreated (total) or pre-extracted (chromatin bound). Cells were then fixed and stained for PARP1. Staining was detected with fluorescent microscopy. Statistical analysis was performed with Welch's *t*-test. (b) HaCat cells were pretreated with the indicated test compounds for 60 min and PARP1 chromatin recruitment was induced with 200-µM H_2O_2 for 60 min. Cells were pre-extracted, fixed and stained for PARP1. A violin plot shows the mean intensity for 1,000 cells per condition. Statistical analysis was performed with Kruskal–Wallis test followed by Dunn's test. (c) HaCat cells transiently transfected with PARP1-mCherry 36–48 h earlier were treated with 10-µM CIP or 10-µM AMO together with 10 µg·ml^{-1} Hoechst 33342 for a period of 30 min. After 40 pre-irradiation images, a point in the nucleus (white arrows) was microirradiated (t = 0) with a confocal microscope equipped with a 405-nm laser and the recruitment of PARP1 to the site of the DNA damage was followed in time. The recruitment (increase in fluorescence intensity above pre-irradiation) was normalized to its maximum value within the observation period of 5 min. The symbols show the mean and SD

(Figure 5b), suggesting that they may act proximally to the DNA binding step. To rule out the possibility that ciclopirox and apomorphine physically interfere with the interaction of PARP1 and DNA breaks, we carried out laser microirradiation experiments. Our data show that PARP1 can efficiently bind to laser-induced DNA breaks in ciclopirox- or apomorphine-pretreated cells with kinetics indistinguishable from untreated cells (Figure 5c). Thus, we concluded that ciclopirox and apomorphine might suppress oxidative DNA damage rather than directly interfering with the interaction of PARP1 and DNA breaks. Indeed, both molecules prevented the

formation of single- and double-stranded DNA breaks, as determined by the comet assay and γH2AX visualization, respectively (Figure 6a,b).

3.7 | Ciclopirox and apomorphine chelate iron and inhibit secondary reactive oxygen species (ROS) production

Since hydrogen peroxide toxicity involves hydroxyl radical production via the Fenton reaction (Grzelak et al., 2018; Jansova et al., 2014), we sought to investigate whether ciclopirox or apomorphine affects this pathway. The fluorogenic dye calcein-AM is a sensitive intracellular iron probe used for monitoring changes in intracellular iron levels (Ma et al., 2015). The acetoxymethyl ester group enables cellular uptake of the probe and, once inside cells, the acetoxymethyl ester group is removed by intracellular esterases. The binding of iron to calcein quenches its fluorescence, whereas iron chelators cause calcein fluorescence dequenching (Ma et al., 2015). We found that under the experimental conditions used throughout this study, H_2O_2 caused an increase in the labile iron pool in HaCat cells (Figure 7a). Both ciclopirox and apomorphine showed a dequenching effect, indicating

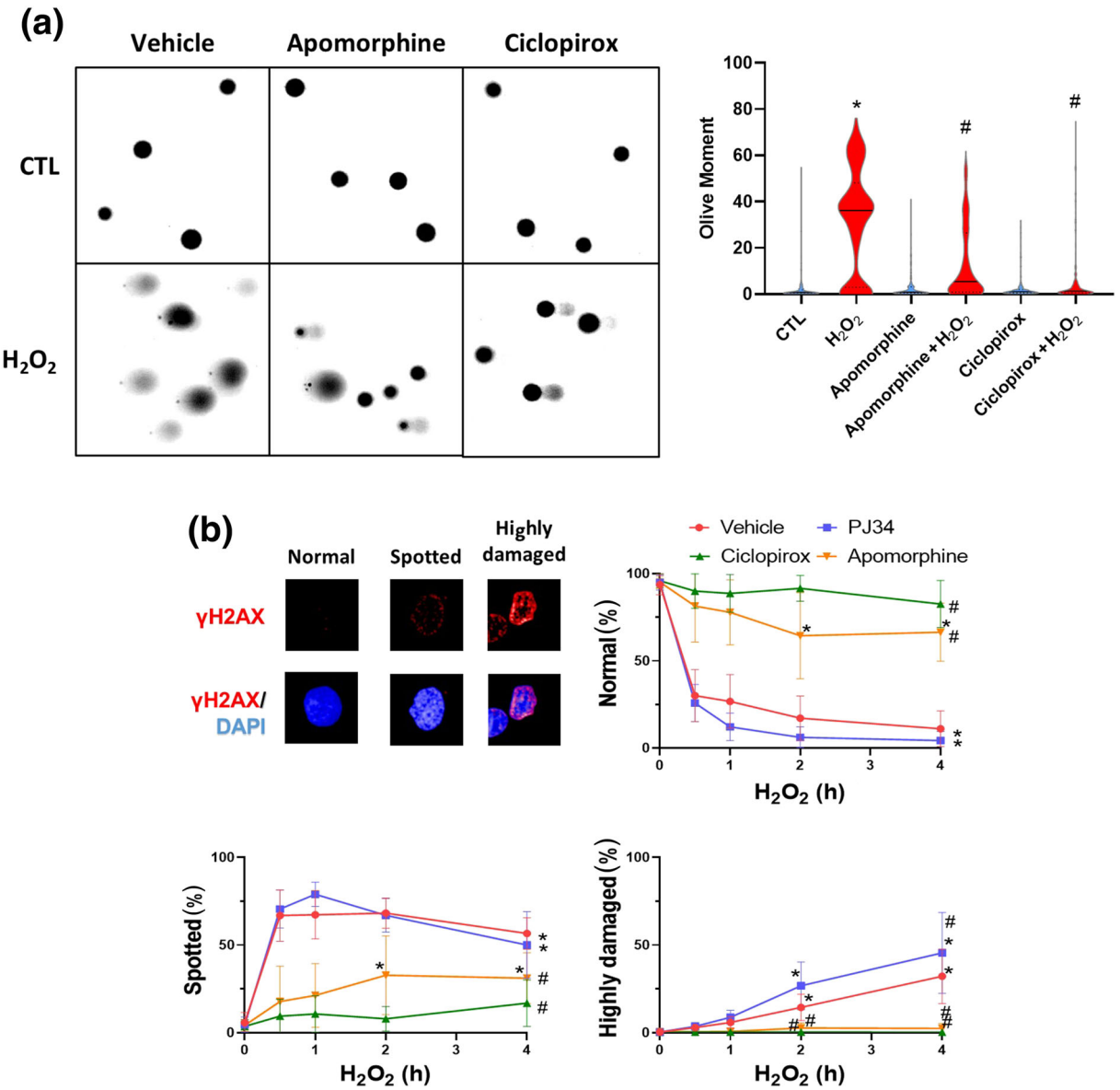

FIGURE 6 Ciclopirox (CIP) and apomorphine (AMO) suppress H_2O_2-induced genotoxicity. (a) HaCat cells were pretreated with the indicated compounds and genotoxicity was induced with 200-μM H_2O_2 for 10 min. An alkaline comet assay was performed. Nuclei were stained with PI and visualized by confocal microscopy. Comets were analysed with OpenComet software. Values of Olive moment are presented in violin plots. Statistical analysis was performed with Kruskal–Wallis test followed by Dunn's test. (b) HaCat cells were pretreated with the indicated compounds and genotoxicity was induced with 200-μM H_2O_2 for the indicated times. Cells were fixed and stained for γH2AX to detect dsDNA breaks with confocal microscopy. Nuclei were classified into three subpopulations and presented as a percentage of the total nuclei count. Line graphs show mean and SD. Statistical analysis was performed with two-way ANOVA followed by Dunnett's test

iron-chelating activity (Figure 7a). However, a slight difference between the effects of ciclopirox and apomorphine could be observed. Apomorphine caused a mild calcein quenching before the addition of H_2O_2 and slowed the kinetics of H_2O_2-induced iron mobilization. Ciclopirox, on the other hand, slightly dequenched calcein fluorescence before the addition of the oxidant and then fully blocked H_2O_2-induced iron mobilization (Figure 7a).

Iron chelation by ciclopirox and apomorphine was expected to suppress secondary cellular reactive oxygen species production in oxidatively stressed cells. Moreover, oxidative stress-induced parthanatos is also characterized by mitochondrial dysfunction including mitochondrial reactive oxygen species production (Virag, Salzman, & Szabo, 1998). In line with this hypothesis, both apomorphine and ciclopirox inhibited reactive oxygen species production (Figure 7b) in H_2O_2-treated cells.

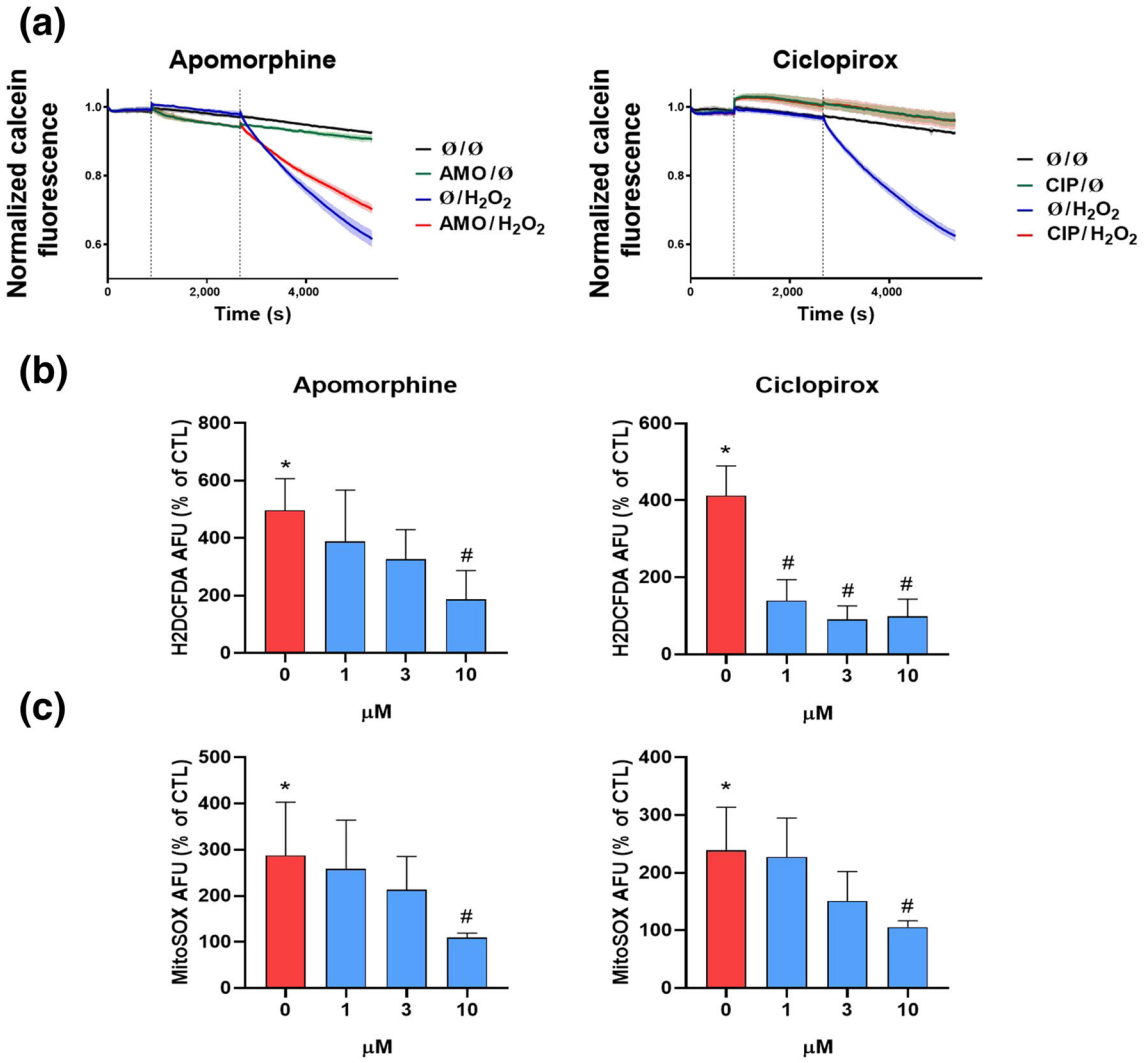

FIGURE 7 Apomorphine (AMO) and ciclopirox (CIP) act as iron chelators and inhibit H_2O_2-induced reactive oxygen species (ROS) production. (a) HaCat cells were incubated with 250-nM calcein-AM in normal culture medium for 1 h. Cells were washed twice with HBSS and then incubated for 30 min to allow the uncleaved calcein-AM to diffuse out of the cells. The medium was changed again, this time to HBSS containing 2.5 $\mu g \cdot ml^{-1}$ propidium iodide and the cells were kept in the incubator for another 30 min to allow the PI to equilibrate between the medium and the cell interior. The plates were placed into a fluorescent plate reader and both the calcein and the PI fluorescence were recorded kinetically. After recording a baseline in the first 15 min, 10-µM CIP or AMO was injected into the designated wells and the dequenching of calcein fluorescence was followed for 30 min. Next, 200-µM H_2O_2 was injected into the designated wells and the quenching of calcein fluorescence by the increasing intracellular labile iron pool was followed for 45 min. The sample marked in red received neither CIP nor H_2O_2. The one in black was not pretreated with CIP before it received the H_2O_2. Finally, the one in blue was pretreated with CIP and H_2O_2. PI exclusion served as a control for the integrity of the plasma membrane to preclude that calcein intensity alterations were due to leakage. Data are presented as mean and SD (n = 5). (b) HaCat cells were pretreated with AMO or CIP for 60 min at the indicated concentrations. Cell death was induced with 200-µM H_2O_2 for 4 h. Intracellular reactive oxygen species (ROS) was measured with H_2DCFDA. Data are presented as mean and SD. (c) HaCat cells were pretreated with AMO or CIP for 60 min at the indicated concentrations. Cell death was induced with 200-µM H_2O_2 for 8 h. Mitochondrial superoxide generation was measured with MitoSOX. Data are presented as mean and SD. H_2O_2 effects were calculated with a Welch's t-test against control. Statistical analysis was performed with one-way ANOVA followed by Dunnett's test

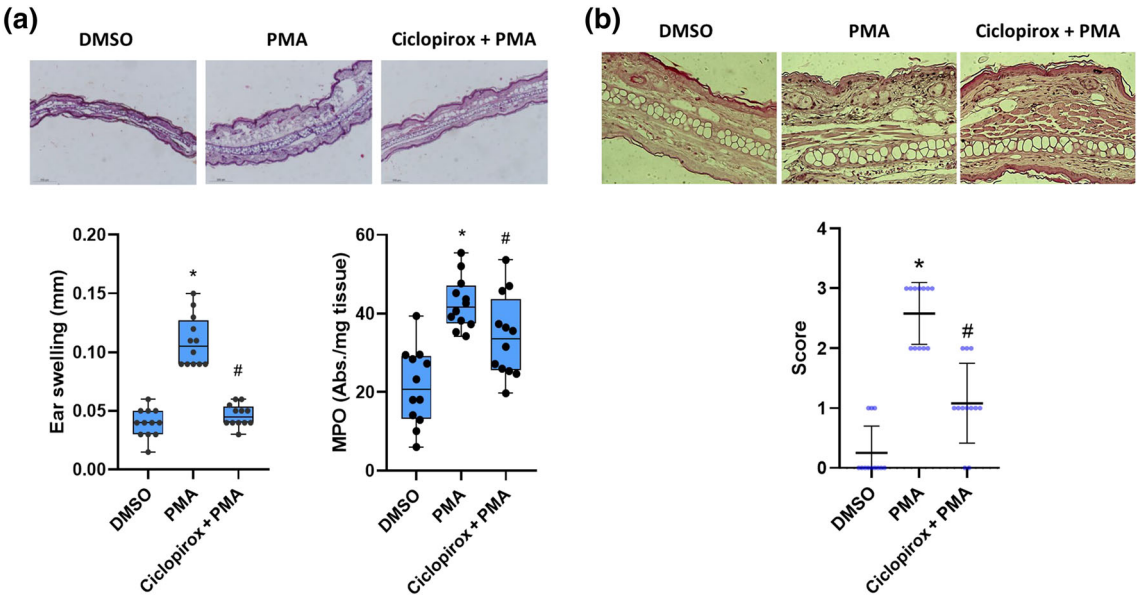

FIGURE 8 Effect of ciclopirox (CIP) on phorbol 12-myristate 13-acetate (PMA)-induced mouse ear swelling and PAR formation. (a) Before the induction of inflammation, the ear thickness of mice was measured with a thickness gauge. Mice were then treated with DMSO or PMA (20 μl per ear applied with a micropipette, 10 μl to each side of the ear). Sixty minutes later, the control and PMA groups were treated with DMSO and the PMA-CIP group was treated with 10-μM CIP (20 μl smeared onto ears with a micropipette, 10 μl to each side of the ear). Six hours after the PMA treatment, the ear thickness was measured again. Box plots show 12 ears per condition. Statistical analysis was performed with Kruskal–Wallis test followed by Dunn's test. Myeloperoxidase (MPO) was measured from ear tissues. Statistical analysis was performed with one-way ANOVA followed by Holm–Sidak test. (b) PAR formation was detected in mouse ears by routine immunohistochemical staining. Images were scored as described in Section 2 and statistical analysis was performed with Fisher's exact test

3.8 | Dermatitis

Since PARP inhibitors have been shown to suppress inflammation in various forms of shock and acute and chronic models of inflammation, we wondered whether our most potent cytoprotective compound, ciclopirox, also possesses anti-inflammatory effects. We applied ciclopirox topically on the skin of mice in a PMA-induced model of dermatitis. Our data show that the drug effectively suppressed oedema (ear swelling) and reduced inflammatory cell migration in this model (Figure 8a). Moreover, in line with previous publications (Bakondi et al., 2019; Gehl et al., 2012; Virag et al., 2002), inflammation-associated PARP activation could be confirmed by the detection of PAR polymer in the skin (Figure 8b). In ciclopirox-treated ears, the PAR level was significantly reduced, suggesting that the drug also acts proximally to PARP activation *in vivo* (Figure 8b).

4 | DISCUSSION

Parthanatotic cell death is a relatively novel cell death modality contributing to tissue injury in various diseases, such as stroke, myocardial ischaemia–reperfusion injury, neurodegenerative diseases and various forms of shock. Since a large set of preclinical data proves that inhibition of PARylation is a viable strategy to protect cells and tissues from oxidative injury, it has been proposed that PARP inhibitor could be repurposed for the treatment of oxidative stress-related pathologies (Berger et al., 2018). Moreover, novel agents are clearly needed to target early events of parthanatos to diversify the therapeutic weaponry to combat these life-threatening conditions.

The high-content screening method presented here represents an effort to identify compounds with anti-parthanatos properties. The aim of the high-content screening was to identify novel parthanatos inhibitors equalling or surpassing the cytoprotective potency of PJ34, a PARP inhibitor that has been extensively tested in oxidative stress-related pathologies (Jagtap et al., 2002). The high (>0.5) Z' factor for this new high-content screening assay indicates an excellent dynamic range and signal variation.

The repurposing screen of a small library of FDA approved drugs yielded several hit compounds. One interesting group of hit compounds includes **phentolamine**, **prazosin** and **formoterol**. These molecules all act on adrenoceptors. Phentolamine and prazosin are α-adrenoceptor antagonists, whereas formoterol is a β_2 receptor agonist.

With regard to formoterol, it is worthwhile mentioning that several other β-receptor agonists have been reported to suppress high mobility group box 1 protein (HMGB1) release by macrophages (Gero et al., 2013). Of note, nuclear-to-cytosolic translocation of HMGB1 during DNA damage-induced necrosis is mediated by PARP1, which thus contributes to the release of this necrotic inflammatory mediator from the cell (Ditsworth et al., 2007). In another study, the β-adrenoceptor antagonist, propranolol, suppressed PARylation in oxidatively stressed U937 cells and leukocytes. Thus, it appears that

β-adrenoceptor signalling converges on PARP, but the effects are context and cell type dependent.

As for the α-adrenoceptor antagonists, phentolamine and prazosin, cytoprotective effects of these drugs have not yet been reported, so it may be worthwhile investigating in the future.

A sizable set of hit compounds included antibiotics and anticancer agents that bind to or intercalate between the two strands of DNA. This set included rifapentine, rifaximin, **primaquine**, **idarubicin**, **doxorubicin**, **mitoxantrone** and epirubicin. We hypothesize that these compounds may interfere with PARP1 recognition of DNA damage and/or PARP1 activation, due to their DNA binding activities. Our data showing that rifaximin did not inhibit PAR synthesis in H_2O_2-treated cells may contradict this hypothesis. It is also possible that these drugs bind PAR polymers and may, thus, interfere with PAR degradation. This latter scenario may also result in cytoprotection (Bakondi et al., 2004; Erdelyi et al., 2009). Follow-up studies may reveal the exact mechanism of the cytoprotective effects of this set of molecules.

Previous studies revealed that parthanatos is doubly intertwined with calcium signalling. On the one hand, calcium signalling is required for PARP1 activation in oxidative stress-induced cell death models (Bakondi et al., 2003; Virag et al., 1999). On the other hand, PARP1 activation also disturbs calcium homeostasis causing distal calcium mobilization events (Burkle & Virag, 2013; Virag, Salzman, & Szabo, 1998). We hypothesize that the cytoprotective effects of the calcium channel blocker, **nisoldipine**, and the PDE inhibitor, **amrinone**, may be related to the interaction between PARylation and calcium signalling. How the two structurally unrelated serotonin reuptake inhibitors, sertraline and fluoxetine, protect cells from oxidative stress-induced cell death remains an enigma.

We carried out the most detailed mechanistic evaluation with two hit compounds: apomorphine and ciclopirox. These two compounds worked similarly, with ciclopirox being more potent in most assays. They blocked H_2O_2-induced PARylation, but their effect was proximal to PARP1. PARP1 binding to oxidatively damaged DNA was inhibited by both compounds whereas binding to methylnitronitrosoguanidine-alkylated DNA was unaffected (data not shown). However, PARP1 recognition and binding to DNA breaks were unaltered, as proven by the laser microirradiation experiments. These data suggest that ciclopirox and apomorphine act by interfering with upstream events of oxidative damage signalling. Indeed, the two drugs prevented single- and double-stranded DNA breakage, as shown in comet assays and γH2AX detection. At this point, we analysed the literature about the known cellular effects of these compounds.

Apomorphine is used primarily as a dopamine receptor agonist for the treatment of Parkinson's disease (Pessoa et al., 2018). The anti-inflammatory effects of dopamine are mediated, at least in part, via β-adrenoceptors (Hasko et al., 2002). This may suggest that the cytoprotective pathways triggered by apomorphine may overlap with those discussed above for β-adrenoceptor agonists. Other dopaminec agonists with similar catechol-based structures, however have also been reported to exert PARP1-independent cytoprotective actions that were unrelated to their dopamine receptor agonist effects (Gero et al., 2007). Catechols have iron-chelating effects (Sanchez et al., 2005) and the classic iron chelator, deferoxamine, was also identified as a hit in our current screen. Moreover, the antifungal agent, ciclopirox, also has iron-chelating effects (Eberhard et al., 2009). Our data demonstrate that both agents chelate iron. A connection between iron mobilization and PARP1-mediated cell death has been reported in intermittent hypoxia-induced cell death in rat cerebellar granule cells (Chiu et al., 2012). Moreover, chelation of other metal ions (e.g. zinc or calcium) also inhibits PARP1 directly or indirectly and, thus, provides cytoprotection (Burkle & Virag, 2013; Hegedus & Virag, 2014; Virag et al., 1999; Virag & Szabo, 1999).

The compartmentalization of cellular iron pools, especially the poorly understood nuclear iron compartment, is an important issue in understanding how ciclopirox and apomorphine work. Apomorphine and ciclopirox likely have access to the nuclear iron pool to prevent DNA damage. Furthermore, oxidative damage is not localized exclusively to the nucleus but causes damage throughout the cell. Mitochondria, which represent an important cellular iron compartment (Ward & Cloonan, 2019), were also damaged under our experimental conditions, as indicated by secondary mitochondrial reactive oxygen species production. It is worthwhile mentioning here that mitochondrial dysfunction and secondary reactive oxygen species production may also be a consequence of PARP activation (Virag et al., 2013; Virag, Salzman, & Szabo, 1998). Thus, the inhibitory effects of ciclopirox and apomorphine on mitochondrial reactive oxygen species production may be either due to mitochondrial iron chelation or due to indirect PARP inhibition via the prevention of oxidative DNA damage.

Inhibition of PARylation protects tissues from injury and suppresses inflammation, as demonstrated in numerous preclinical models (Virag & Szabo, 2002). Here, we tested whether the indirect inhibitory actions of ciclopirox on PARP also translate into anti-inflammatory effects in acute dermatitis. In line with previous data demonstrating activation of PARP1 in skin inflammation (Bakondi et al., 2002; El-Hamoly et al., 2014; Szabo et al., 2001), we demonstrated increased PAR polymer levels in the inflamed ears of mice. Ciclopirox suppressed inflammation and inhibited PAR formation. These results indicate that the anti-inflammatory effects of ciclopirox are also due to interference with PARP proximal signalling events, most likely iron chelation and the consequent reduction in hydroxyl radical production. Moreover, the prevention of PARP activation by ciclopirox likely reduces the level of automodified PARP1, which is known as a co-activator for the inflammatory transcription factor NF-κB. To what extent inhibition of inflammatory cell death or NF-κB signalling contributes to the anti-inflammatory action of ciclopirox and whether ciclopirox may also have beneficial effects in models of severe tissue injury require further investigation.

It has not escaped our attention that cell death in our model depends largely on both PARP activity and iron mobilization. Thus, hydrogen-peroxide-induced cell death of HaCat cells (and likely other cell types) shares features of both parthanatos and ferroptosis. Dual involvement of these two pathways would not be unprecedented, as it has been described in glutamate-induced excitotoxic neuronal cell

death (Dixon et al., 2012). PARylation has also been shown to contribute to various cell death modalities (Virag et al., 2013). However, it would go beyond the scope of this paper to provide a detailed characterization of all cell death pathways potentially involved in our model.

In summary, we developed and tested a high-content analysis assay to identify molecules inhibiting parthanatotic cell death. Even in a rather small drug library, we found several compounds that suppressed H_2O_2-induced parthanatos. Two of the most potent cytoprotective hits (ciclopirox and apomorphine) protect by chelating iron, thus preventing hydroxyl radical-mediated DNA breakage. A series of follow-up studies may reveal the mechanisms of additional hits identified in our screen and clarify whether any of these compounds can be repurposed for the treatment of tissue injuries or inflammation.

ACKNOWLEDGEMENTS

L.V. received funding from the National Research, Development and Innovation Office grants GINOP-2.3.2-15-2016-00020 TUMORDNS, GINOP-2.3.2-15-2016-00048-STAYALIVE, OTKA K132193 and OTKA K112336. C.H. received funding from the National Research, Development and Innovation Office grant OTKA PD116845 and Bolyai postdoctoral fellowship (Hungarian Academy of Sciences, BO/00468/17/8) and was supported by the ÚNKP-19-4-DE-299 New National Excellence Program of the Ministry of Human Capacities. The authors are grateful for the careful English language editing by Dr. Karen Uray and for help with statistical evaluation of data by Dr. Eszter Janka.

AUTHOR CONTRIBUTIONS

Z.R. planned and performed experiments for Figures 1–7 and did the statistical analysis. M.A.D. planned and performed experiments for Figures 5 and 7. K.K. planned and performed experiments for Figure 6. Z.H. and M.N.-P. planned and performed experiments for Figure 8. E.B. planned and performed experiments for Figures 3 and 7. A.K. performed experiments for Figure 1. C.H. planned and performed experiments for Figure 1 and wrote the manuscript. L.V. obtained funding, designed and organized the study, and wrote the manuscript.

CONFLICT OF INTEREST

The authors declare no conflicts of interest.

DECLARATION OF TRANSPARENCY AND SCIENTIFIC RIGOUR

This Declaration acknowledges that this paper adheres to the principles for transparent reporting and scientific rigour of preclinical research as stated in the *BJP* guidelines for Design & Analysis, Immunoblotting and Immunochemistry and Animal Experimentation, and as recommended by funding agencies, publishers and other organizations engaged with supporting research.

DATA AVAILABILITY STATEMENT

The data that support the findings of this study are available from the corresponding author upon reasonable request. Some data may not be made available because of privacy or ethical restrictions.

REFERENCES

Alexander, S. P. H., Roberts, R. E., Broughton, B. R. S., Sobey, C. G., George, C. H., Stanford, S. C., … Ahluwalia, A. (2018). Goals and practicalities of immunoblotting and immunohistochemistry: A guide for submission to the *British Journal of Pharmacology*. *British Journal of Pharmacology*, *175*, 407–411. https://doi.org/10.1111/bph.14112

Alexander, S. P. H., Christopoulos, A., Davenport, A. P., Kelly, E., Mathie, A., Peters, J. A., … Pawson, A. J. (2019a). The Concise Guide to PHARMACOLOGY 2019/20: G protein-coupled receptors. *British Journal of Pharmacology*, *176*(Suppl 1), S21–S141. https://doi.org/10.1111/bph.14748

Alexander, S. P. H., Christopoulos, A., Davenport, A. P., Kelly, E., Mathie, A., Peters, J. A., … Pawson, A. J. (2019b). The Concise Guide to PHARMACOLOGY 2019/20: G protein-coupled receptors. *British Journal of Pharmacology*, *176*(Suppl 1), S21–S141. https://doi.org/10.1111/bph.14748

Andrabi, S. A., Dawson, T. M., & Dawson, V. L. (2008). Mitochondrial and nuclear cross talk in cell death: Parthanatos. *Annals of the New York Academy of Sciences*, *1147*, 233–241. https://doi.org/10.1196/annals.1427.014

Bakondi, E., Bai, P., Erdelyi, K., Szabo, C., Gergely, P., & Virag, L. (2004). Cytoprotective effect of gallotannin in oxidatively stressed HaCaT keratinocytes: The role of poly(ADP-ribose) metabolism. *Experimental Dermatology*, *13*, 170–178. https://doi.org/10.1111/j.0906-6705.2004.0150.x

Bakondi, E., Bai, P., Szabo, E. E., Hunyadi, J., Gergely, P., Szabo, C., & Virág, L. (2002). Detection of poly(ADP-ribose) polymerase activation in oxidatively stressed cells and tissues using biotinylated NAD substrate. *The Journal of Histochemistry and Cytochemistry*, *50*, 91–98. https://doi.org/10.1177/002215540205000110

Bakondi, E., Gonczi, M., Szabo, E., Bai, P., Pacher, P., Gergely, P., … Virág, L. (2003). Role of intracellular calcium mobilization and cell-density-dependent signaling in oxidative-stress-induced cytotoxicity in HaCaT keratinocytes. *The Journal of Investigative Dermatology*, *121*, 88–95. https://doi.org/10.1046/j.1523-1747.2003.12329.x

Bakondi, E., Singh, S. B., Hajnady, Z., Nagy-Penzes, M., Regdon, Z., Kovacs, K., … Demény, M. Á. (2019). Spilanthol inhibits inflammatory transcription factors and iNOS expression in macrophages and exerts anti-inflammatory effects in dermatitis and pancreatitis. *International Journal of Molecular Sciences*, *20*, 4308. https://doi.org/10.3390/ijms20174308

Berger, N. A., Besson, V. C., Boulares, A. H., Burkle, A., Chiarugi, A., Clark, R. S., … Haskó, G. (2018). Opportunities for the repurposing of PARP inhibitors for the therapy of non-oncological diseases. *British Journal of Pharmacology*, *175*, 192–222. https://doi.org/10.1111/bph.13748

Borbely, A., Toth, A., Edes, I., Virag, L., Papp, J. G., Varro, A., … Papp, Z. (2005). Peroxynitrite-induced alpha-actinin nitration and contractile alterations in isolated human myocardial cells. *Cardiovascular Research*, *67*, 225–233. https://doi.org/10.1016/j.cardiores.2005.03.025

Brunyanszki, A., Hegedus, C., Szanto, M., Erdelyi, K., Kovacs, K., Schreiber, V., … Bai, P. (2010). Genetic ablation of PARP-1 protects against oxazolone-induced contact hypersensitivity by modulating oxidative stress. *The Journal of Investigative Dermatology*, *130*, 2629–2637. https://doi.org/10.1038/jid.2010.190

Burkle, A., & Virag, L. (2013). Poly(ADP-ribose): PARadigms and PARadoxes. *Molecular Aspects of Medicine*, *34*, 1046–1065. https://doi.org/10.1016/j.mam.2012.12.010

Chiu, S. C., Huang, S. Y., Tsai, Y. C., Chen, S. P., Pang, C. Y., Lien, C. F., … Yang, K. T. (2012). Poly(ADP-ribose) polymerase plays an important role in intermittent hypoxia-induced cell death in rat cerebellar granule cells. *Journal of Biomedical Science*, *19*, 29–38. https://doi.org/10.1186/1423-0127-19-29

Curtin, N. (2014). PARP inhibitors for anticancer therapy. *Biochemical Society Transactions*, *42*, 82–88. https://doi.org/10.1042/BST20130187

Curtis, M. J., Alexander, S., Cirino, G., Docherty, J. R., George, C. H., Giembycz, M. A., … Ahluwalia, A. (2018). Experimental design and analysis and their reporting II: Updated and simplified guidance for authors and peer reviewers. *British Journal of Pharmacology*, *175*, 987–993. https://doi.org/10.1111/bph.14153

Dawson, T. M., & Dawson, V. L. (2018). Nitric oxide signaling in neurodegeneration and cell death. *Advances in Pharmacology*, *82*, 57–83. https://doi.org/10.1016/bs.apha.2017.09.003

Ditsworth, D., Zong, W. X., & Thompson, C. B. (2007). Activation of poly(ADP)-ribose polymerase (PARP-1) induces release of the pro-inflammatory mediator HMGB1 from the nucleus. *The Journal of Biological Chemistry*, *282*, 17845–17854. https://doi.org/10.1074/jbc.M701465200

Dixon, S. J., Lemberg, K. M., Lamprecht, M. R., Skouta, R., Zaitsev, E. M., Gleason, C. E., … Stockwell, B. R. (2012). Ferroptosis: An iron-dependent form of nonapoptotic cell death. *Cell*, *149*, 1060–1072. https://doi.org/10.1016/j.cell.2012.03.042

Douglas, D. L., & Baines, C. P. (2014). PARP1-mediated necrosis is dependent on parallel JNK and Ca^{2+}/calpain pathways. *Journal of Cell Science*, *127*, 4134–4145. https://doi.org/10.1242/jcs.128009

Droge, W. (2002). Free radicals in the physiological control of cell function. *Physiological Reviews*, *82*, 47–95. https://doi.org/10.1152/physrev.00018.2001

Eberhard, Y., McDermott, S. P., Wang, X., Gronda, M., Venugopal, A., Wood, T. E., … Antholine, W. E. (2009). Chelation of intracellular iron with the antifungal agent ciclopirox olamine induces cell death in leukemia and myeloma cells. *Blood*, *114*, 3064–3073. https://doi.org/10.1182/blood-2009-03-209965

El-Hamoly, T., Hegedus, C., Lakatos, P., Kovacs, K., Bai, P., El-Ghazaly, M. A., … Virág, L. (2014). Activation of poly(ADP-ribose) polymerase-1 delays wound healing by regulating keratinocyte migration and production of inflammatory mediators. *Molecular Medicine*, *20*, 363–371. https://doi.org/10.2119/molmed.2014.00130

Erdelyi, K., Bai, P., Kovacs, I., Szabo, E., Mocsar, G., Kakuk, A., … Virág, L. (2009). Dual role of poly(ADP-ribose) glycohydrolase in the regulation of cell death in oxidatively stressed A549 cells. *The FASEB Journal*, *23*, 3553–3563. https://doi.org/10.1096/fj.09-133264

Gehl, Z., Bai, P., Bodnar, E., Emri, G., Remenyik, E., Nemeth, J., … Szabó, É. (2012). Poly(ADP-ribose) in the skin and in melanomas. *Histology and Histopathology*, *27*, 651–659. https://doi.org/10.14670/HH-27.651

Gero, D., Modis, K., Nagy, N., Szoleczky, P., Toth, Z. D., Dorman, G., & Szabó, C. (2007). Oxidant-induced cardiomyocyte injury: Identification of the cytoprotective effect of a dopamine 1 receptor agonist using a cell-based high-throughput assay. *International Journal of Molecular Medicine*, *20*, 749–761.

Gero, D., Szoleczky, P., Modis, K., Pribis, J. P., Al-Abed, Y., Yang, H., … Szabo, C. (2013). Identification of pharmacological modulators of HMGB1-induced inflammatory response by cell-based screening. *PLoS ONE*, *8*, e65994. https://doi.org/10.1371/journal.pone.0065994

Greenwald, S. H., & Pierce, E. A. (2019). Parthanatos as a cell death pathway underlying retinal disease. *Advances in Experimental Medicine and Biology*, *1185*, 323–327. https://doi.org/10.1007/978-3-030-27378-1_53

Grzelak, A., Wojewodzka, M., Meczynska-Wielgosz, S., Zuberek, M., Wojciechowska, D., & Kruszewski, M. (2018). Crucial role of chelatable iron in silver nanoparticles induced DNA damage and cytotoxicity. *Redox Biology*, *15*, 435–440. https://doi.org/10.1016/j.redox.2018.01.006

Hasko, G., Szabo, C., Nemeth, Z. H., & Deitch, E. A. (2002). Dopamine suppresses IL-12 p40 production by lipopolysaccharide-stimulated macrophages via a β-adrenoceptor-mediated mechanism. *Journal of Neuroimmunology*, *122*, 34–39. https://doi.org/10.1016/S0165-5728(01)00459-3

Hegedus, C., Lakatos, P., Olah, G., Toth, B. I., Gergely, S., Szabó, C., & Virág, L. (2008). Protein kinase C protects from DNA damage-induced necrotic cell death by inhibiting poly(ADP-ribose) polymerase-1. *FEBS Letters*, *582*, 1672–1678. https://doi.org/10.1016/j.febslet.2008.04.023

Hegedus, C., & Virag, L. (2014). Inputs and outputs of poly(ADP-ribosyl)ation: Relevance to oxidative stress. *Redox Biology*, *2*, 978–982. https://doi.org/10.1016/j.redox.2014.08.003

Jagtap, P., Soriano, F. G., Virág, L., Liaudet, L., Mabley, J., Szabó, É., … Szabó, C. (2002). Novel phenanthridinone inhibitors of poly(adenosine 5′-diphosphate-ribose) synthetase: Potent cytoprotective and anti-shock agents*. *Critical Care Medicine*, *30*(5), 1071–1082. https://doi.org/10.1097/00003246-200205000-00019

Jang, K. H., Do, Y. J., Son, D., Son, E., Choi, J. S., & Kim, E. (2017). AIF-independent parthanatos in the pathogenesis of dry age-related macular degeneration. *Cell Death & Disease*, *8*, e2526.

Jansova, H., Machacek, M., Wang, Q., Haskova, P., Jirkovska, A., Potuckova, E., … Šimůnek, T. (2014). Comparison of various iron chelators and prochelators as protective agents against cardiomyocyte oxidative injury. *Free Radical Biology & Medicine*, *74*, 210–221. https://doi.org/10.1016/j.freeradbiomed.2014.06.019

Kers, J., Leemans, J. C., & Linkermann, A. (2016). An overview of pathways of regulated necrosis in acute kidney injury. *Seminars in Nephrology*, *36*, 139–152. https://doi.org/10.1016/j.semnephrol.2016.03.002

Kovacs, K., Erdelyi, K., Hegedus, C., Lakatos, P., Regdon, Z., Bai, P., … Virág, L. (2012). Poly(ADP-ribosyl)ation is a survival mechanism in cigarette smoke-induced and hydrogen peroxide-mediated cell death. *Free Radical Biology & Medicine*, *53*, 1680–1688. https://doi.org/10.1016/j.freeradbiomed.2012.08.579

Lilley, E., Stanford, S. C., Kendall, D. E., Alexander, S. P., Cirino, G., Docherty, J. R., … Ahluwalia, A. (2020). ARRIVE 2.0 and the *British Journal of Pharmacology*: Updated guidance for 2020. *British Journal of Pharmacology*, *177*(16), 3611–3616. https://doi.org/10.1111/bph.15178

Lipinski, B. (2011). Hydroxyl radical and its scavengers in health and disease. *Oxidative Medicine and Cellular Longevity*, *2011*, 809696.

Ma, Y., Abbate, V., & Hider, R. C. (2015). Iron-sensitive fluorescent probes: Monitoring intracellular iron pools. *Metallomics*, *7*, 212–222. https://doi.org/10.1039/C4MT00214H

Majno, G., & Joris, I. (1995). Apoptosis, oncosis, and necrosis. An overview of cell death. *The American Journal of Pathology*, *146*, 3–15.

Michelena, J., Lezaja, A., Teloni, F., Schmid, T., Imhof, R., & Altmeyer, M. (2018). Analysis of PARP inhibitor toxicity by multidimensional fluorescence microscopy reveals mechanisms of sensitivity and resistance. *Nature Communications*, *9*, 2678–2694. https://doi.org/10.1038/s41467-018-05031-9

Murai, J., Huang, S. Y., Das, B. B., Renaud, A., Zhang, Y., Doroshow, J. H., … Pommier, Y. (2012). Trapping of PARP1 and PARP2 by clinical PARP inhibitors. *Cancer Research*, *72*, 5588–5599. https://doi.org/10.1158/0008-5472.CAN-12-2753

Nakajima, H., Nagaso, H., Kakui, N., Ishikawa, M., Hiranuma, T., & Hoshiko, S. (2004). Critical role of the automodification of poly(ADP-ribose) polymerase-1 in nuclear factor-κB-dependent gene expression in primary cultured mouse glial cells. *Journal of Biological Chemistry*, *279*, 42774–42786.

Percie du Sert, N., Hurst, V., Ahluwalia, A., Alam, S., Avey, M. T., Baker, M., … Würbel, H. (2020). The ARRIVE guidelines 2.0: Updated guidelines for reporting animal research. *PLoS Biology*, *18*(7), e3000410. https://doi.org/10.1371/journal.pbio.3000410

Pessoa, R. R., Moro, A., Munhoz, R. P., Teive, H. A. G., & Lees, A. J. (2018). Apomorphine in the treatment of Parkinson's disease: A review. *Arquivos de Neuro-Psiquiatria*, *76*, 840–848. https://doi.org/10.1590/0004-282x20180140

Rack, J. G. M., Palazzo, L., & Ahel, I. (2020). (ADP-ribosyl)hydrolases: Structure, function, and biology. *Genes & Development*, *34*, 263–284. https://doi.org/10.1101/gad.334631.119

Regdon, Z., Robaszkiewicz, A., Kovacs, K., Rygielska, Z., Hegedus, C., Bodoor, K., … Virág, L. (2019). LPS protects macrophages from AIF-independent parthanatos by downregulation of PARP1 expression, induction of SOD2 expression, and a metabolic shift to aerobic glycolysis. *Free Radical Biology & Medicine*, *131*, 184–196. https://doi.org/10.1016/j.freeradbiomed.2018.11.034

Robinson, N., Ganesan, R., Hegedus, C., Kovacs, K., Kufer, T. A., & Virag, L. (2019). Programmed necrotic cell death of macrophages: Focus on pyroptosis, necroptosis, and parthanatos. *Redox Biology*, *26*, 101239. https://doi.org/10.1016/j.redox.2019.101239

Sanchez, P., Galvez, N., Colacio, E., Minones, E., & Dominguez-Vera, J. M. (2005). Catechol releases iron(III) from ferritin by direct chelation without iron(II) production. *Dalton Transactions*, 811–813. https://doi.org/10.1039/B416669H

Szabo, E., Virag, L., Bakondi, E., Gyure, L., Hasko, G., Bai, P., … Szabó, C. (2001). Peroxynitrite production, DNA breakage, and poly(ADP-ribose) polymerase activation in a mouse model of oxazolone-induced contact hypersensitivity. *The Journal of Investigative Dermatology*, *117*, 74–80. https://doi.org/10.1046/j.0022-202x.2001.01388.x

Vanden Berghe, T., Linkermann, A., Jouan-Lanhouet, S., Walczak, H., & Vandenabeele, P. (2014). Regulated necrosis: The expanding network of non-apoptotic cell death pathways. *Nature Reviews. Molecular Cell Biology*, *15*, 135–147. https://doi.org/10.1038/nrm3737

Virag, L., Robaszkiewicz, A., Rodriguez-Vargas, J. M., & Oliver, F. J. (2013). Poly(ADP-ribose) signaling in cell death. *Molecular Aspects of Medicine*, *34*, 1153–1167. https://doi.org/10.1016/j.mam.2013.01.007

Virag, L., Salzman, A. L., & Szabo, C. (1998). Poly(ADP-ribose) synthetase activation mediates mitochondrial injury during oxidant-induced cell death. *Journal of Immunology*, *161*, 3753–3759.

Virag, L., Scott, G. S., Antal-Szalmas, P., O'Connor, M., Ohshima, H., & Szabo, C. (1999). Requirement of intracellular calcium mobilization for peroxynitrite-induced poly(ADP-ribose) synthetase activation and cytotoxicity. *Molecular Pharmacology*, *56*, 824–833.

Virag, L., Scott, G. S., Cuzzocrea, S., Marmer, D., Salzman, A. L., & Szabo, C. (1998). Peroxynitrite-induced thymocyte apoptosis: The role of caspases and poly(ADP-ribose) synthetase (PARS) activation. *Immunology*, *94*, 345–355. https://doi.org/10.1046/j.1365-2567.1998.00534.x

Virag, L., & Szabo, C. (1999). Inhibition of poly(ADP-ribose) synthetase (PARS) and protection against peroxynitrite-induced cytotoxicity by zinc chelation. *British Journal of Pharmacology*, *126*, 769–777. https://doi.org/10.1038/sj.bjp.0702332

Virag, L., & Szabo, C. (2002). The therapeutic potential of poly(ADP-ribose) polymerase inhibitors. *Pharmacological Reviews*, *54*, 375–429. https://doi.org/10.1124/pr.54.3.375

Virag, L., Szabo, E., Bakondi, E., Bai, P., Gergely, P., Hunyadi, J., & Szabó, C. (2002). Nitric oxide-peroxynitrite-poly(ADP-ribose) polymerase pathway in the skin. *Experimental Dermatology*, *11*, 189–202. https://doi.org/10.1034/j.1600-0625.2002.110301.x

Virag, L., Szabo, E., Gergely, P., & Szabo, C. (2003). Peroxynitrite-induced cytotoxicity: Mechanism and opportunities for intervention. *Toxicology Letters*, *140-141*, 113–124. https://doi.org/10.1016/S0378-4274(02)00508-8

Wang, Y., An, R., Umanah, G. K., Park, H., Nambiar, K., Eacker, S. M., … Dawson, T. M. (2016). A nuclease that mediates cell death induced by DNA damage and poly(ADP-ribose) polymerase-1. *Science*, *354*, aad6872. https://doi.org/10.1126/science.aad6872

Ward, D. M., & Cloonan, S. M. (2019). Mitochondrial iron in human health and disease. *Annual Review of Physiology*, *81*, 453–482. https://doi.org/10.1146/annurev-physiol-020518-114742

Yu, S. W., Wang, H., Poitras, M. F., Coombs, C., Bowers, W. J., Federoff, H. J., … Dawson, V. L. (2002). Mediation of poly(ADP-ribose) polymerase-1-dependent cell death by apoptosis-inducing factor. *Science*, *297*, 259–263. https://doi.org/10.1126/science.1072221

Zhang, J. H., Chung, T. D., & Oldenburg, K. R. (1999). A simple statistical parameter for use in evaluation and validation of high throughput screening assays. *Journal of Biomolecular Screening*, *4*, 67–73. https://doi.org/10.1177/108705719900400206

SUPPORTING INFORMATION

Additional supporting information may be found online in the Supporting Information section at the end of this article.

How to cite this article: Regdon Z, Demény MA, Kovács K, et al. High-content screening identifies inhibitors of oxidative stress-induced parthanatos: cytoprotective and anti-inflammatory effects of ciclopirox. *Br J Pharmacol*. 2021;178:1095–1113. https://doi.org/10.1111/bph.15344